Data report: atlas of lithic grain types at Site C0002; reference for petrographic provenance analysis in the Kumano Basin and upper Nankai accretionary prism[1]

Sebastian G. Ramirez[2] and Kitty L. Milliken[3]

Chapter contents

[1] Ramirez, S.G., and Milliken, K.L., 2016. Data report: atlas of lithic grain types at Site C0002; reference for petrographic provenance analysis in the Kumano Basin and upper Nankai accretionary prism. *In* Strasser, M., Dugan, B., Kanagawa, K., Moore, G.F., Toczko, S., Maeda, L., and the Expedition 338 Scientists, *Proceedings of the Integrated Ocean Drilling Program,* 338: Yokohama (Integrated Ocean Drilling Program). doi:10.2204/iodp.proc.338.204.2016
[2] Institute of Geophysics, Jackson School of Geosciences, University of Texas at Austin, Austin TX 78712, USA. Correspondence author: sgramirez@utexas.edu
[3] Bureau of Economic Geology, Jackson School of Geosciences, University of Texas at Austin, Austin TX 78713, USA.

Abstract

Sand samples collected during Integrated Ocean Drilling Program Expeditions 338 and 315 at Site C0002 show a variety of lithic fragment types. The lithic component in these sediments includes grains of sedimentary, metamorphic, volcanic, and plutonic origin. An atlas of lithic grain types from Site C0002 serves as a useful reference for petrographic provenance analysis in the Kumano Basin and the underlying prism sediments. The relative abundance of monocrystalline mineral grains and grain ratios are subject to textural and diagenetic controls external to provenance. Lithic grains, in particular, provide very specific and reliable information on variations in sediment source.

Introduction

Lithic grains are polycrystalline particles that can in many cases be identified as belonging to specific parent lithologies. Although monocrystalline grains may have internal textures (e.g., Bernet and Bassett, 2005; Lee et al., 1998), the provenance information in monocrystalline grains (quartz, feldspar, and dense minerals) is primarily derived from their composition, which for feldspars and dense minerals can be modified by dissolution and replacement during diagenesis (e.g., Milliken and Mack, 1990; Milliken, 1988; Morton, 1984). Grain ratios (e.g., quartz-feldspar-lithic fragments) are also subject to control by grain size (Ingersoll et al., 1984), a factor that is not fully removed even by the Gazzi-Dickinson point-count technique that extracts large monocrystals from lithic grains (Milliken et al., 2012; Decker and Helmold, 1985). In lithic fragments themselves, however, provenance information resides mostly in their textures, which are less subject to post-depositional alteration (Milliken, 1988) and unaffected by grain size once a grain is sufficiently large to preserve the texture. Lithic grains are "recognizable fragments of the source terrane" (Decker and Helmold, 1985) and as such constitute an easily accessible and exceptionally reliable type of information on sediment source. Survival of lithic grains during sediment transport is favored in far-distal sands that avoid reworking in coastal depositional systems (Dutton and Loucks, 2010).

The atlas presented here intends to serve as a reference for the lithic grain types observed within the sand-size (62 µm to 2 mm) grain fraction of the Kumano Basin and underlying Nankai accre-

doi:10.2204/iodp.proc.338.204.2016

tionary prism. Our grain identifications draw on materials presented in several published petrography resources (Usman et al., 2014; Fergusson, 2011; Milliken et al., 2007; Underwood and Fergusson, 2005; Fergusson, 2003; Garzanti and Vezzoli, 2003; Marsaglia, 1992; Marsaglia et al., 1992; De Rosa et al., 1986; Taira and Niitsuma, 1986; Scholle, 1979).

Methods and materials

Core and cuttings sandy sediment samples (10 cm^3) were collected through the basin and prism stratigraphy during Integrated Ocean Drilling Program (IODP) Expedition 338 (**Strasser et al.,** 2014). Where possible, intervals with no sample coverage were completed with material recovered during IODP Expedition 315 (see the "Expedition 315 Site C0002" chapter [Expedition 315 Scientists, 2009]). Sampling distribution was ~1 sample per core/cuttings where available. A total of 99 Miocene–recent samples were obtained.

Semiconsolidated sediments of each sample were fully disaggregated with the help of a sonicator and were wet-sieved using 62 µm mesh to isolate the sand-size fraction. Dried sand was impregnated with blue-dyed epoxy and mounted into thin sections. Each sample was stained following the method outlined by Houghton (1980), in which Ca-plagioclase is stained pink, K-feldspar is stained yellow, glass may take one or both colors, and Na-plagioclase remains unstained.

Each sample was studied under a transmitted-light microscope (plane- and cross-polarized modes), and photomicrographs of representative lithic fragments were taken. Unless otherwise indicated, the grain of interest is at the center of the image.

Results

A total of 162 photomicrographs are included (Figs. **F1, F2, F3, F4, F5, F6, F7, F8, F9, F10, F11, F12, F13, F14, F15, F16, F17, F18, F19, F20, F21, F22, F23, F24, F25, F26, F27**). The sample number, lithic type, and lithostratigraphic unit of each photographed grain are included in Table **T1.** Lithic grains were grouped into sedimentary lithic fragments (SRFs) (Figs. **F1, F2, F3, F4, F5, F6, F7, F8, F9**), volcanic lithic fragments (VRFs) (Figs. **F10, F11, F12, F13, F14, F15**), plutonic lithic fragments (PRFs) (Figs. **F16, F17, F18, F19**), and metamorphic lithic fragments (MRFs) (Figs. **F20, F21, F22, F23, F24, F25**). SRFs were further divided into clay-rich (Figs. **F1, F2, F3, F4, F5**) and silt-rich (Figs. **F6, F7A–F7D**) mudstones, sandstones (Fig. **F7E–F7F**), argillaceous cherts (Fig. **F8**), and cherts (Fig. **F9**). VRFs were divided into felsitic (Figs. **F10, F11**), microlitic (Fig. **F12**), lathwork (Fig. **F13**), trachytic lathwork (Fig. **F14**), and pumice (Fig. **F15**). PRFs, with the exception of K-feldspar-quartz intergrowths (Fig. **F18**), were not divided. MRFs were divided into quartz rich (Fig. **F20**), quartz-mica rich (Fig. **F21**), micaceous (Fig. **F22**), chlorite rich (Fig. **F23**), epidote rich (Fig. **F24**), and others (Fig. **F25**). Petrographic definitions of each of these lithic fragment categories can be found in Marsaglia (1992), Marsaglia et al. (2013), and Milliken et al. (2007).

Grains that are not lithic fragments, such as poorly disaggregated muds (Fig. **F26**) or postdrilling sulfate precipitates (Fig. **F27**) were included under the category Artifacts.

Acknowledgments

The Integrated Ocean Drilling Program provided the samples used for this report. Postexpedition funding awarded to S.G. Ramirez by the Consortium for Ocean Leadership helped support this project. S.G. Ramirez and K.L. Milliken also wish to thank the Expedition 338 Scientists for their help with shipboard sampling.

References

Bernet, M., and Bassett, K., 2005. Provenance analysis by single-quartz-grain SEM-CL/optical microscopy. *Journal of Sedimentary Research*, 75(3):492–500. **http://dx.doi.org/10.2110/jsr.2005.038**

De Rosa, R., Zuffa, G.G., Taira, A., and Leggett, J.K., 1986. Petrography of trench sands from the Nankai Trough, southwest Japan: implications for long-distance turbidite transportation. *Geological Magazine,* 123(5):477–486. **http://dx.doi.org/10.1017/S0016756800035068**

Decker, J., and Helmold, K.P., 1985. The effect of grain size on detrital modes: a test of the Gazzi-Dickinson point-counting method: discussion. *Journal of Sedimentary Research*, 55(4):618–620. **http://archives.datapages.com/data/sepm/journals/v55-58/data/055/055004/0618.htm**

Dutton, S.P., and Loucks, R.G., 2010. Diagenetic controls on evolution of porosity and permeability in lower Tertiary Wilcox sandstones from shallow to ultradeep (200–6700 m) burial, Gulf of Mexico Basin, U.S.A. *Marine and Petroleum Geology*, 27(1):69–81. **http://dx.doi.org/10.1016/j.marpetgeo.2009.08.008**

Expedition 315 Scientists, 2009. Expedition 315 Site C0002. *In* Kinoshita, M., Tobin, H., Ashi, J., Kimura, G., Lallemant, S., Screaton, E.J., Curewitz, D., Masago, H., Moe, K.T., and the Expedition 314/315/316 Scientists, *Proceedings of the Integrated Ocean Drilling Program,* 314/315/316: Washington, DC (Integrated Ocean Drilling Program Management International, Inc.). **http://dx.doi.org/10.2204/iodp.proc.314315316.124.2009**

Fergusson, C.L., 2003. Provenance of Miocene–Pleistocene turbidite sands and sandstones, Nankai Trough, Ocean Drilling Program Leg 190. *In* Mikada, H., Moore, G.F., Taira, A., Becker, K., Moore, J.C., and Klaus, A. (Eds.), *Proceedings of the Ocean Drilling Program, Scientific Results,* 190/196: College Station, TX (Ocean Drilling Program), 1–28. **http://dx.doi.org/10.2973/odp.proc.sr.190196.205.2003**

Fergusson, C.L., 2011. Data report: clast counts and petrography of gravels from Site C0007, IODP Expedition 316, Nankai Trough. *In* Kinoshita, M., Tobin, H., Ashi, J., Kimura, G., Lallemant, S., Screaton, E.J., Curewitz, D., Masago, H., Moe, K.T., and the Expedition 314/315/316 Scientists, *Proceedings of the Integrated Ocean Drilling Program,* 314/315/316: Washington, DC (Integrated Ocean Drilling Program Management International, Inc.). **http://dx.doi.org/10.2204/iodp.proc.314315316.203.2011**

Garzanti, E., and Vezzoli, G., 2003. A classification of metamorphic grains in sands based on their composition and grade. *Journal of Sedimentary Research*, 73(5):830–837. **http://dx.doi.org/10.1306/012203730830**

Houghton, H.F., 1980. Refined techniques for staining plagioclase and alkali feldspars in thin section. *Journal of Sedimentary Research,* 50(2):629–631. **http://jsedres.geoscienceworld.org/content/50/2/629.abstract**

Ingersoll, R.V., Bullard, T.F., Ford, R.L., Grimm, J.P., Pickle, J.D., and Sares, S.W., 1984. The effect of grain size on detrital modes: a test of the Gazzi-Dickinson point-counting method. *Journal of Sedimentary Research,* 54(1):103–116. **http://dx.doi.org/10.1306/212F83B9-2B24-11D7-8648000102C1865D**

Lee, M.R., Hodson, M.E., and Parsons, I., 1998. The role of intragranular microtextures and microstructures in chemical and mechanical weathering: direct comparisons of experimentally and naturally weathered alkali feldspars. *Geochimica et Cosmochimica Acta*, 62(16):2771–2788. **http://dx.doi.org/10.1016/S0016-7037(98)00200-2**

Marsaglia, K., Milliken, K., and Doran, L., 2013. IODP digital reference for smear slide analysis of marine mud, Part 1: Methodology and atlas of siliciclastic and volcanogenic components. *Integrated Ocean Drilling Program Technical Note,* 1. **http://dx.doi.org/10.2204/iodp.tn.1.2013**

Marsaglia, K.M., 1992. Petrography and provenance of volcaniclastic sands recovered from the Izu-Bonin arc, Leg 126. *In* Taylor, B., Fujioka, K., et al., *Proceedings of the Ocean Drilling Program, Scientific Results,* 126: College Station, TX (Ocean Drilling Program), 139–154. **http://dx.doi.org/10.2973/odp.proc.sr.126.124.1992**

Marsaglia, K.M., Ingersoll, R.V., and Packer, B.M., 1992. Tectonic evolution of the Japanese Islands as reflected in modal compositions of Cenozoic forearc and backarc sand and sandstone. *Tectonics,* 11(5):1028–1044. **http://dx.doi.org/10.1029/91TC03183**

Milliken, K.L., 1988. Loss of provenance information through subsurface diagenesis in Plio-Pleistocene sandstones, northern Gulf of Mexico. *Journal of Sedimentary Research,* 58(6):992–1002. **http://dx.doi.org/10.1306/212F8EE0-2B24-11D7-8648000102C1865D**

Milliken, K.L., Choh, S.-J., and McBride, E.F., 2007. *Sandstone Petrology: A Tutorial Petrographic Image Atlas*, (2nd edition) [CD-ROM]. AAPG/Datapages Discovery Series, 10. **http://store.aapg.org/**

Milliken, K.L., Comer, E.E., and Marsaglia, K.M., 2012. Data report: modal sand composition at Sites C0004, C0006, C0007, and C0008, IODP Expedition 316, Nankai accretionary prism. *In* Kinoshita, M., Tobin, H., Ashi, J., Kimura, G., Lallemant, S., Screaton, E.J., Curewitz, D., Masago, H., Moe, K.T., and the Expedition 314/315/316 Scientists, *Proceedings of the Integrated Ocean Drilling Program,* 314/315/316: Washington, DC (Integrated Ocean Drilling Program Management International, Inc.). **http://dx.doi.org/10.2204/iodp.proc.314315316.221.2012**

Milliken, K.L., and Mack, L.E., 1990. Subsurface dissolution of heavy minerals, Frio Formation sandstones of the ancestral Rio Grande Province, South Texas. *Sedimentary Geology*, 68(3):187–199. **http://dx.doi.org/10.1016/0037-0738(90)90111-6**

Morton, A.C., 1984. Stability of detrital heavy minerals in Tertiary sandstones from the North Sea Basin. *Clay Minerals*, 19(3):287–308. **http://dx.doi.org/10.1180/claymin.1984.019.3.04**

Scholle, P.A., 1979. A color illustrated guide to constituents, textures, cements and porosities of sandstones and associated rocks. AAPG *Memoir,* 28.

Simpson, G.D.H., 2010. Formation of accretionary prisms influenced by sediment subduction and supplied by sediments from adjacent continents. *Geology,* 38(2):131–134. **http://dx.doi.org/10.1130/G30461.1**

Strasser, M., Dugan, B., Kanagawa, K., Moore, G.F., Toczko, S., Maeda, L., Kido, Y., Moe, K.T., Sanada, Y., Esteban, L., Fabbri, O., Geersen, J., Hammerschmidt, S., Hayashi, H., Heirman, K., Hüpers, A., Jurado Rodriguez, M.J., Kameo, K., Kanamatsu, T., Kitajima, H., Masuda, H., Milliken, K., Mishra, R., Motoyama, I., Olcott, K., Oohashi, K., Pickering, K.T., Ramirez, S.G., Rashid, H., Sawyer, D., Schleicher, A., Shan, Y., Skarbek, R., Song, I., Takeshita, T., Toki, T., Tudge, J., Webb, S., Wilson, D.J., Wu, H.-Y., and Yamaguchi, A., 2014. Site C0002. *In* Strasser, M., Dugan, B., Kanagawa, K., Moore, G.F., Toczko, S., Maeda, L., and the Expedition 338 Scientists, *Proceedings of the Integrated Ocean Drilling Program,* 338: Yokohama (Integrated Ocean Drilling Program). **http://dx.doi.org/10.2204/iodp.proc.338.103.2014**

Taira, A., and Niitsuma, N., 1986. Turbidite sedimentation in the Nankai Trough as interpreted from magnetic fabric, grain size, and detrital modal analyses. *In* Kagami, H., Karig, D.E., Coulbourn, W.T., et al., *Initial Reports of the Deep Sea Drilling Project,* 87: Washington, DC (U.S. Govt. Printing Office), 611–632. **http://dx.doi.org/10.2973/dsdp.proc.87.112.1986**

Underwood, M.B., and Fergusson, C.L., 2005. Late Cenozoic evolution of the Nankai trench-slope system: Evidence from sand petrography and clay mineralogy. *In* Hodgson, D., and Flint, S. (Eds.), *Submarine Slope Sys-*

tems: Processes, Products and Prediction. Geological Society Special Publication, 244(1):113–129. **http://dx.doi.org/10.1144/GSL.SP.2005.244.01.07**

Usman, M.O., Masago, H., Winkler, W., and Strasser, M., 2014. Mid-Quaternary decoupling of sediment routing in the Nankai forearc revealed by provenance analysis of turbiditic sands. *International Journal of Earth Sciences*, 103(4):1141–1161. **http://dx.doi.org/10.1007/s00531-014-1011-z**

Initial receipt: 14 September 2015
Acceptance: 30 November 2015
Publication: 16 February 2016
MS 338-204

Figure F1. Sedimentary rock fragments: clay-rich mudstones. Grains rich in clay-size clay minerals with minor admixtures of possible organic matter and opaque crystals such as pyrite. Left = plane-polarized light, right = cross-polarized light.

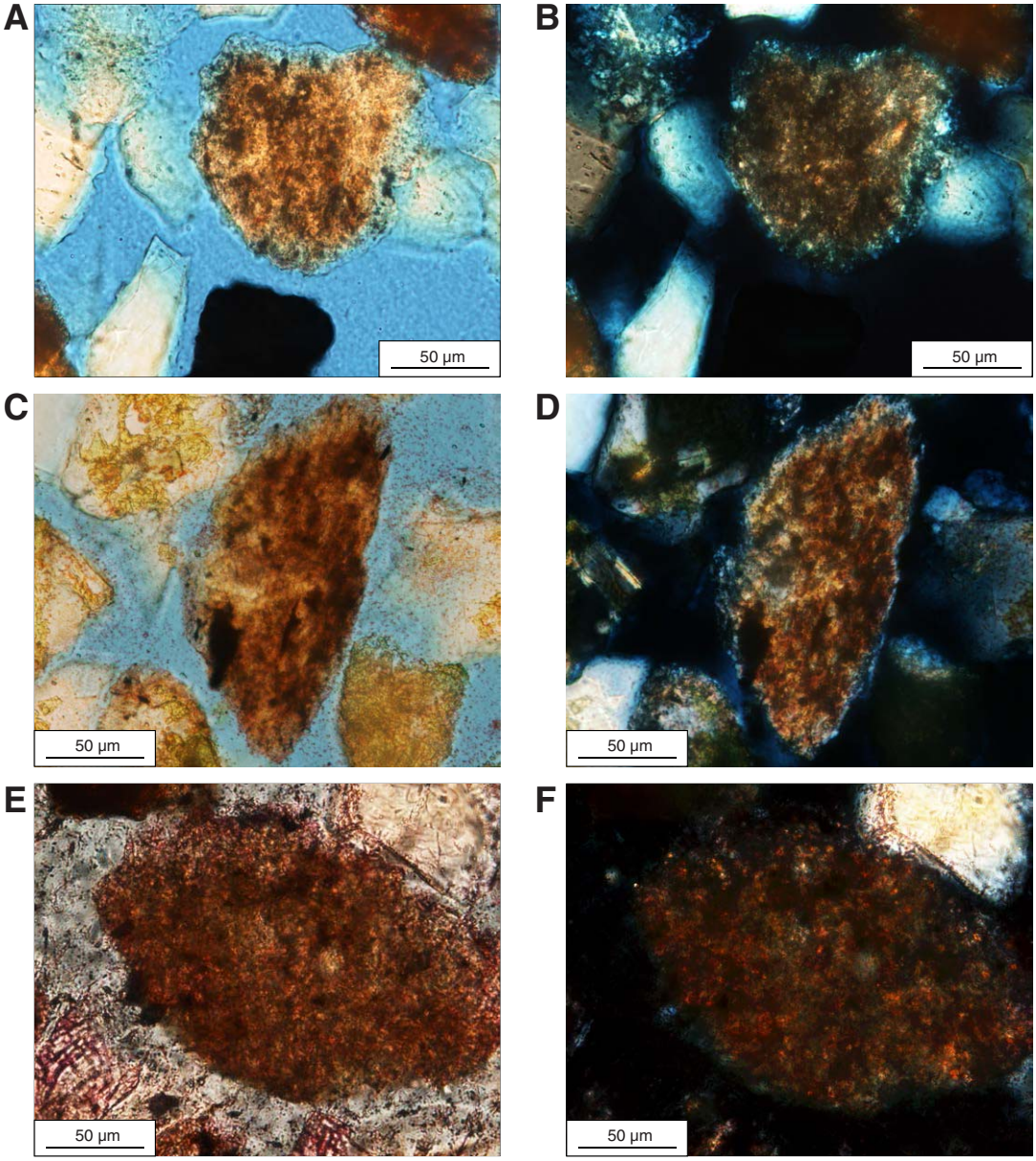

Figure F2. Sedimentary rock fragments: clay-rich mudstones. Grains rich in clay-size clay minerals with minor admixtures of possible organic matter and opaque crystals such as pyrite. Bottom grain (E, F) contains a moderate amount of clay-size carbonate. Left = plane-polarized light, right = cross-polarized light.

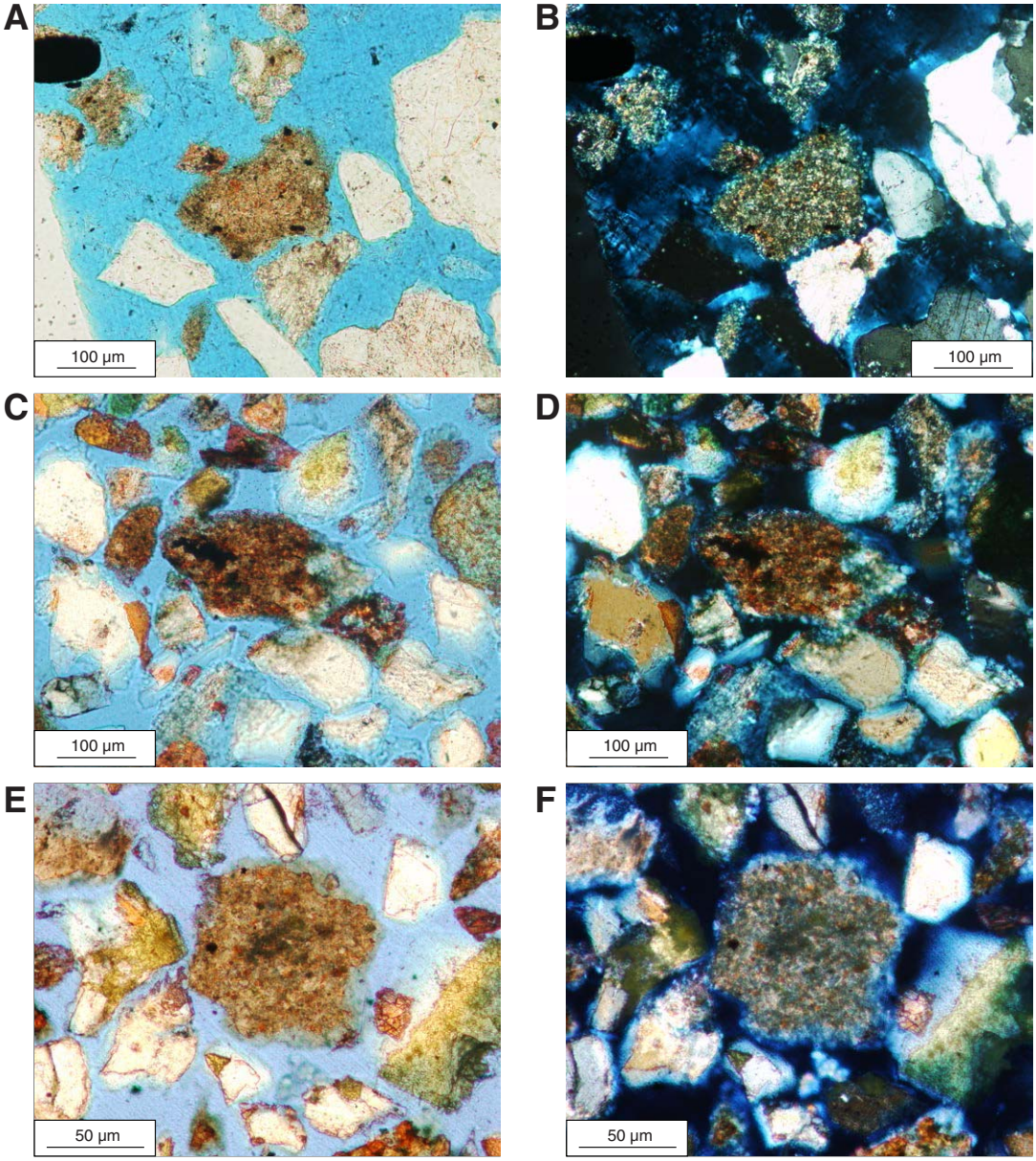

Figure F3. Sedimentary rock fragments: clay-rich mudstones. Color zoning in these samples is likely the result of varying degrees of epoxy penetration during the thin section making process. This interpretation is based upon the similarity to variable epoxy impregnation commonly observed in whole-rock mudstone thin sections. Left = plane-polarized light, right = cross-polarized light.

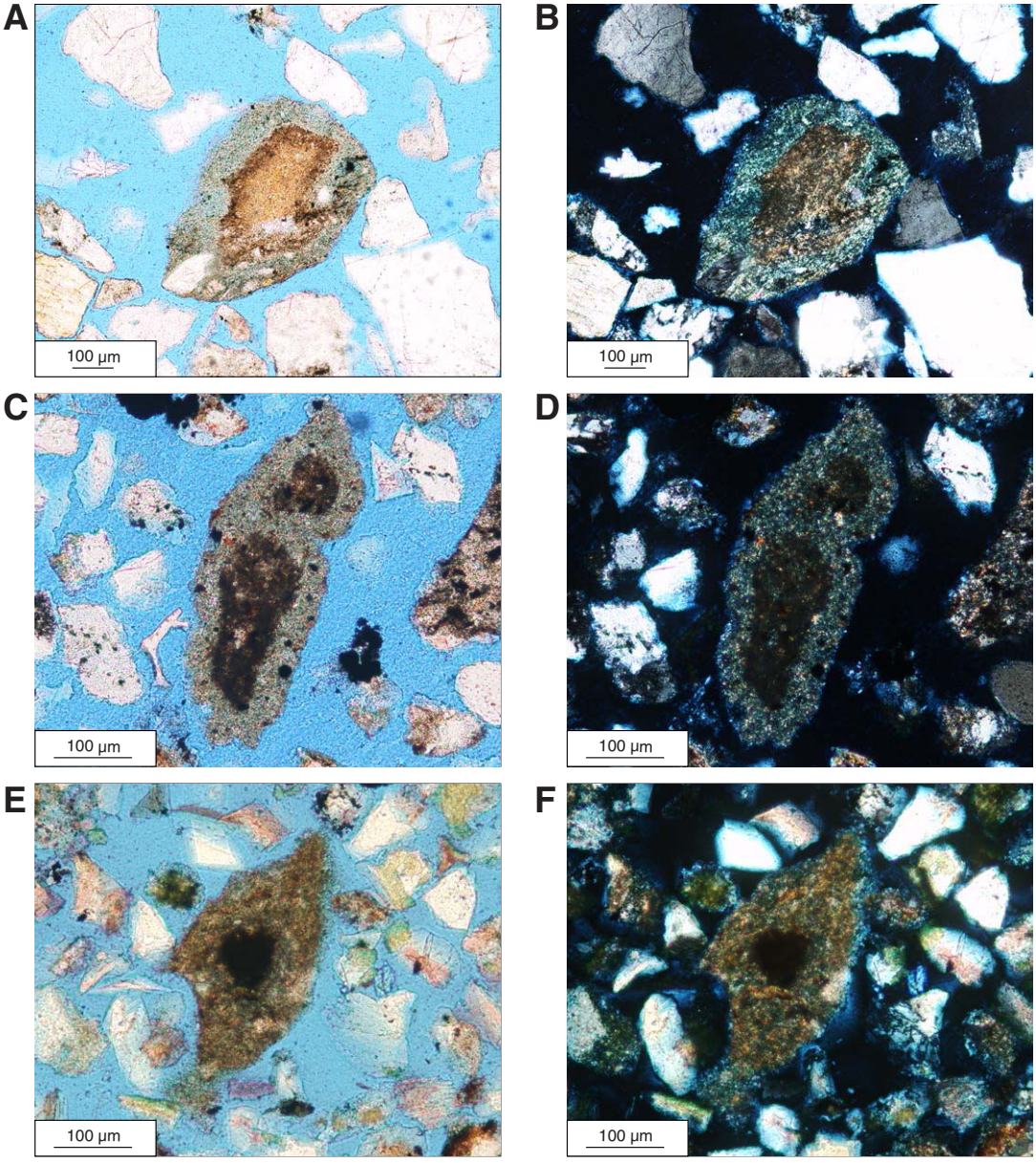

Figure F4. Sedimentary rock fragments: clay-rich mudstones. **A, B.** Grain has fractures filled with microcrystalline quartz (chert). **C, D.** Near-opaque grain has fracture filled with chlorite. Grain in lower right has a chert-filled fracture. **E, F.** Clay-rich mudstone grain containing a sand-size quartz clast. Left = plane-polarized light, right = cross-polarized light.

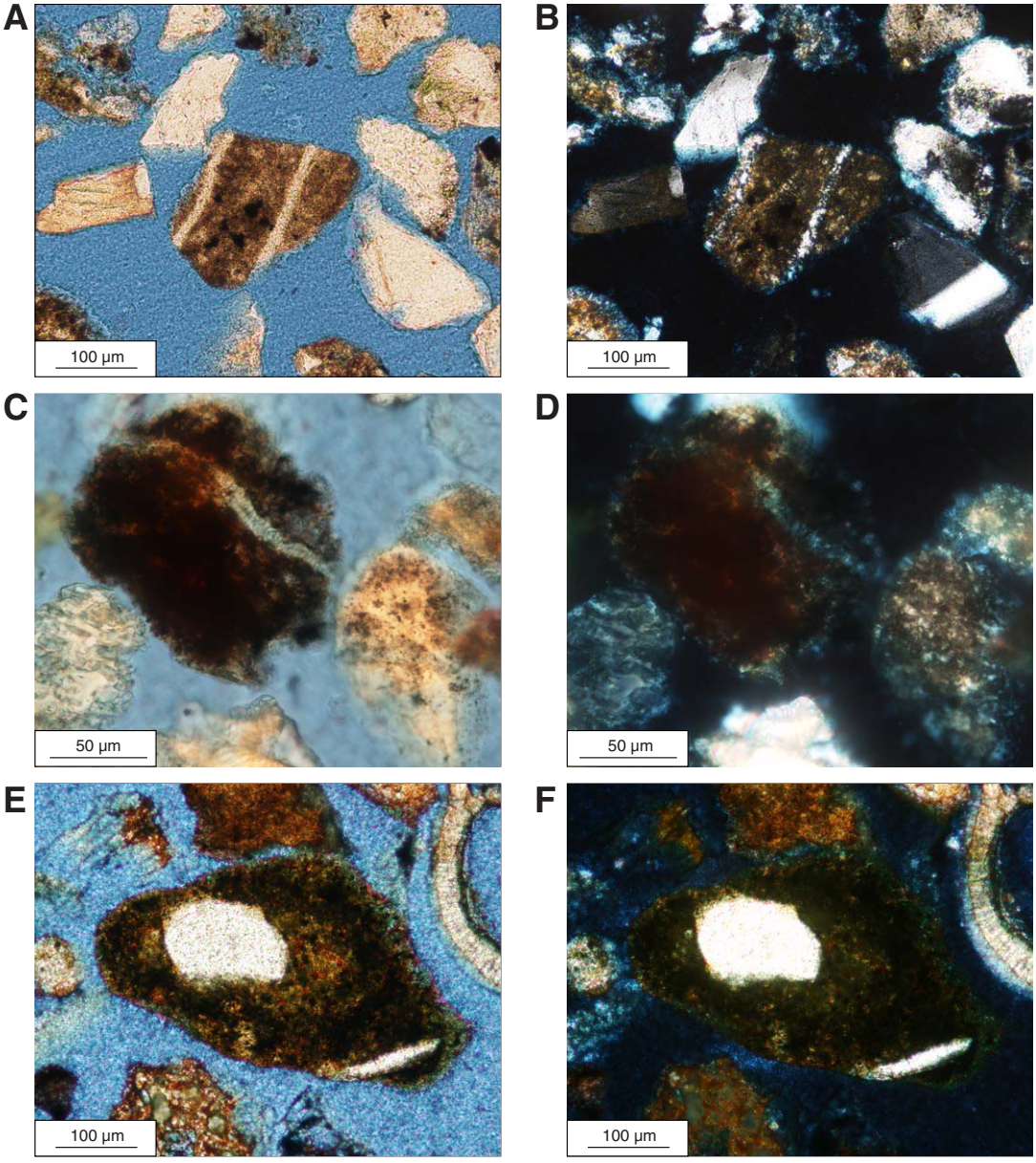

Figure F5. Sedimentary rock fragments: clay-rich mudstones. Silt-size particles are quartz and feldspar. Mudstones are silt bearing. Left = plane-polarized light, right = cross-polarized light.

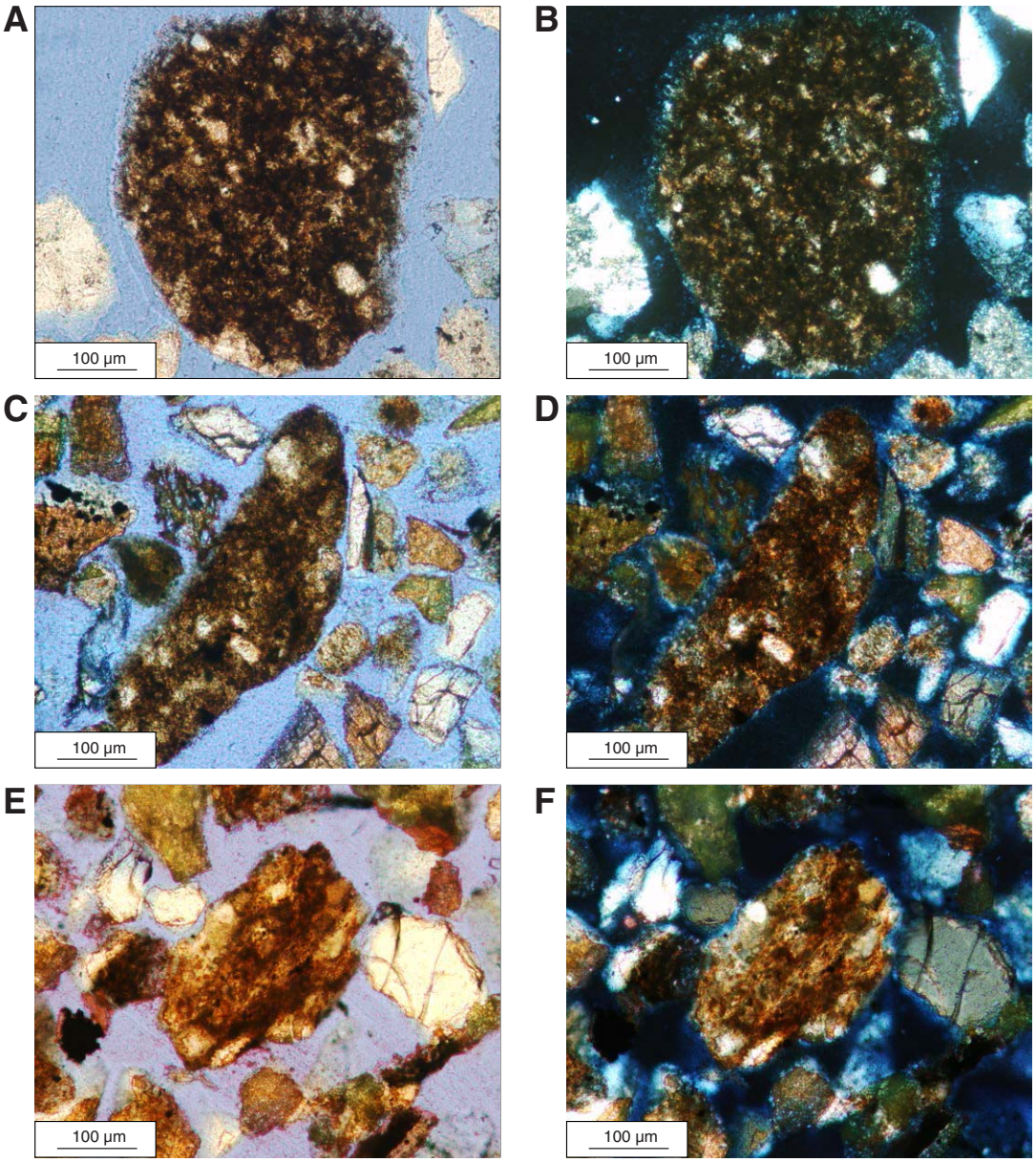

Figure F6. Sedimentary rock fragments: silt-rich mudstones. Silt-size particles are quartz and feldspar. Left = plane-polarized light, right = cross-polarized light.

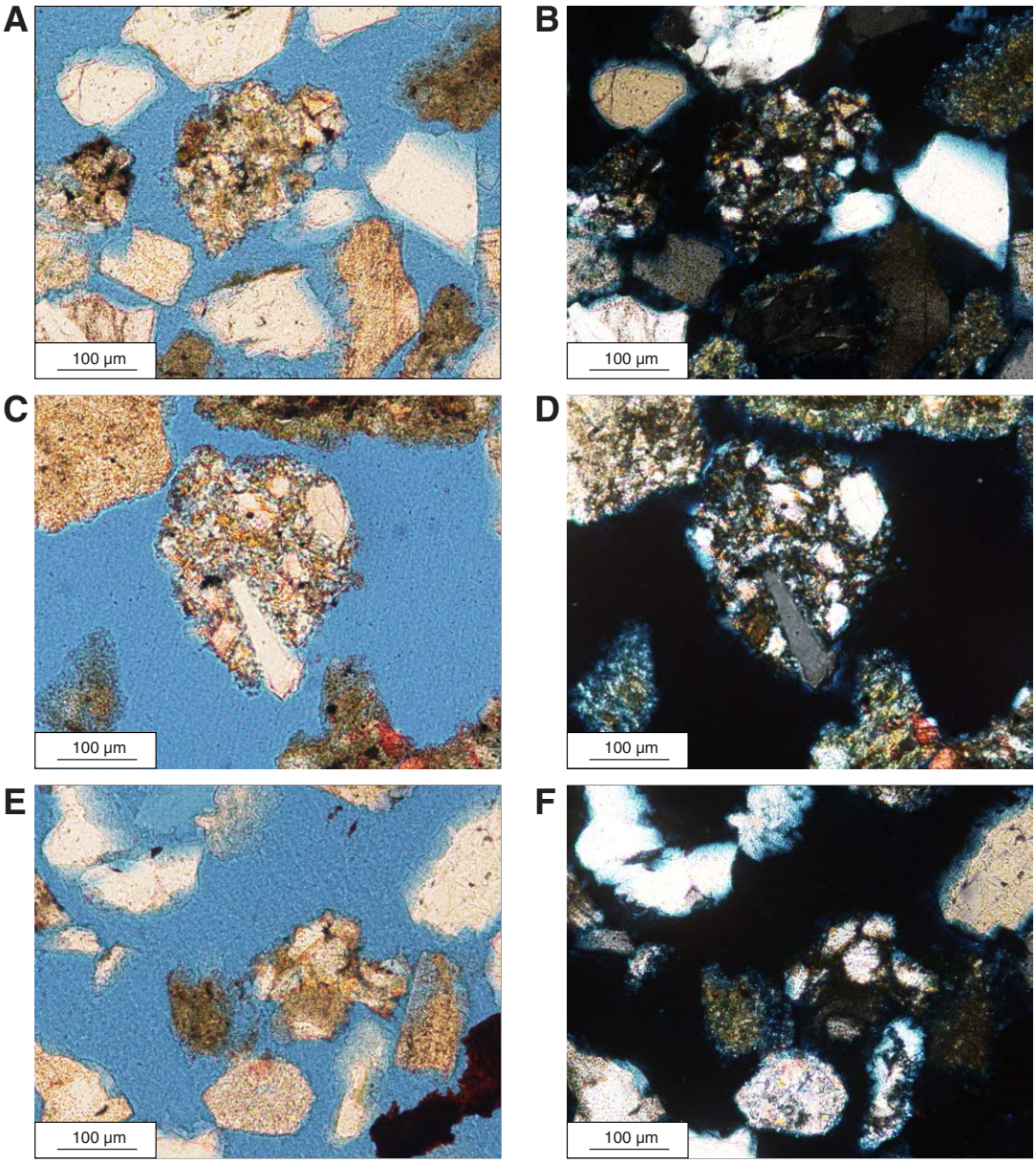

Figure F7. Sedimentary rock fragments: silt-rich mudstones. **A–D.** Mudstones (silt-rich). **E, F.** Muddy sandstone. Large sand-size grain; on right side is a metamorphic rock fragment composed of quartz, feldspar and chlorite. Smaller grains include quartz and feldspar. Left = plane-polarized light, right = cross-polarized light.

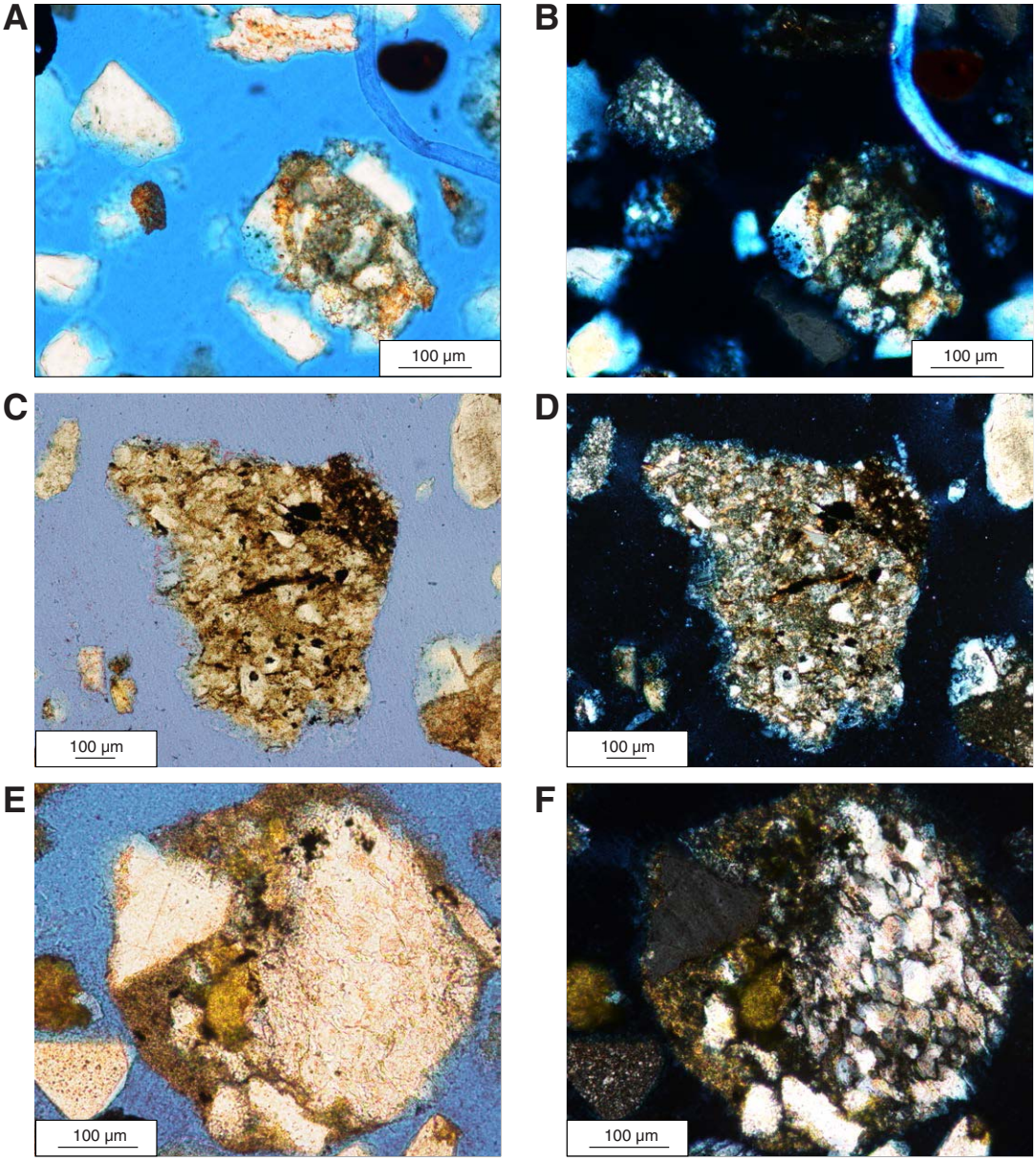

Figure F8. Sedimentary rock fragments: argillaceous cherts. **A, B.** Opaque crystals are probably pyrite. Left = plane-polarized light, right = cross-polarized light.

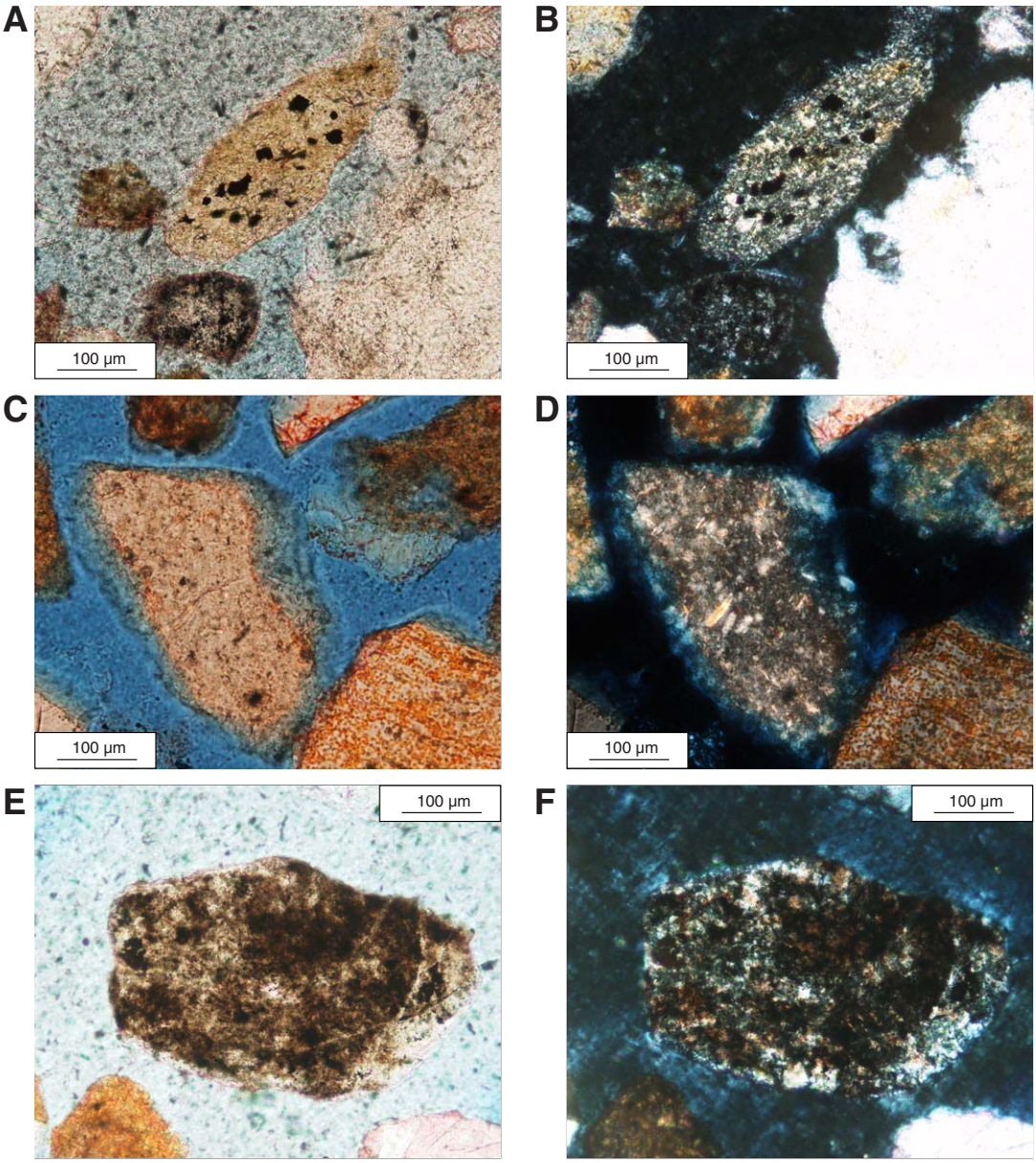

Figure F9. Sedimentary rock fragments: cherts and other microcrystalline quartz. **A, B.** Fine grained. **C, D.** Well-rounded grain, potentially formed within a vesicle of a volcanic rock fragment (Fig. F15E–F15F). While not strictly sedimentary, this grain is interpreted to have formed through water-rock interaction similar in nature to diagenesis. **E, F.** Oversized grain with fractures filled with microcrystalline quartz. Left = plane-polarized light, right = cross-polarized light.

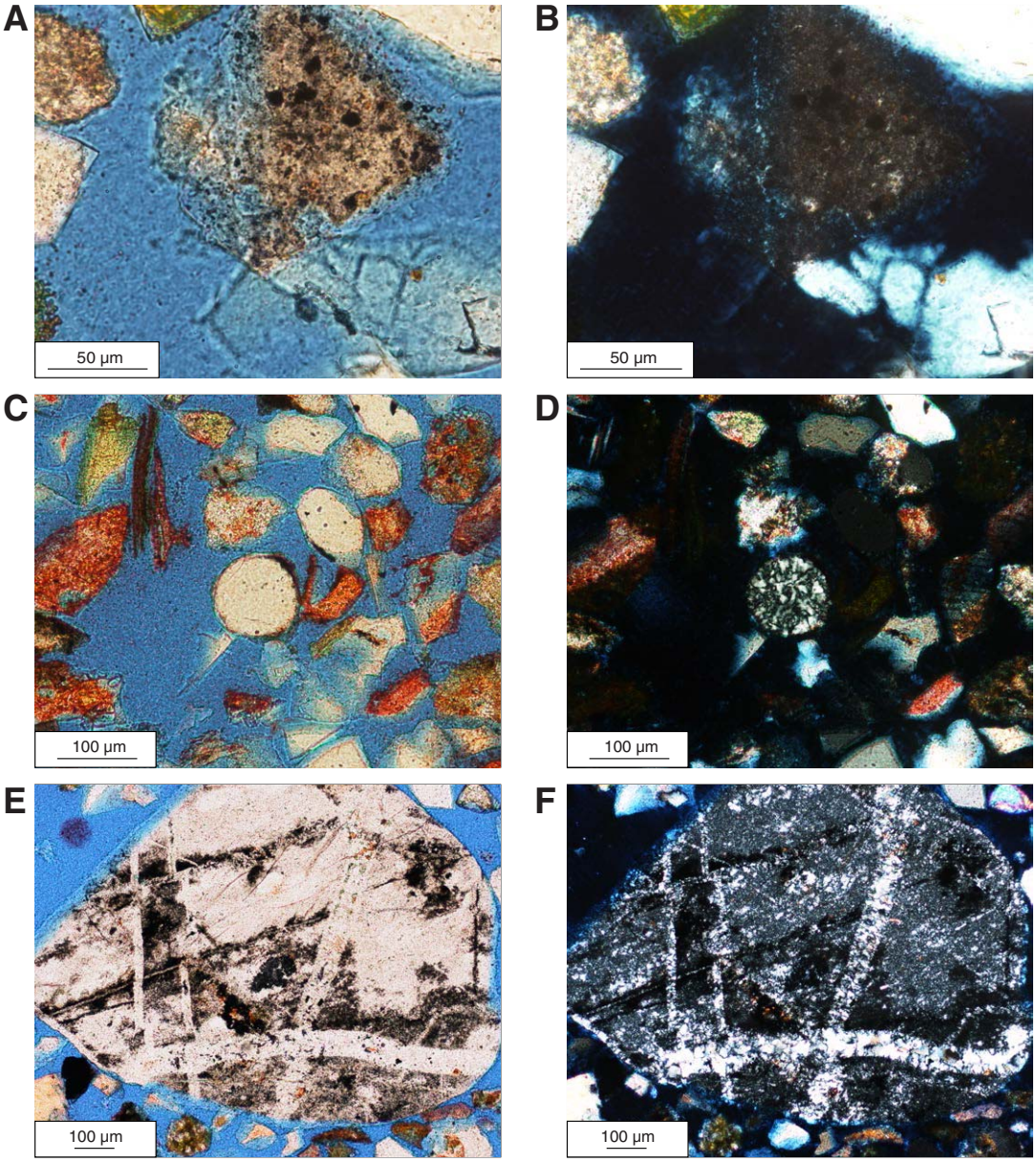

Figure F10. Volcanic rock fragments: felsitic grains are characterized by microcrystalline quartz and feldspar crystals of equant dimensions. The presence of abundant feldspar is denoted by the prominent yellow stain. These grains also contain a substantial admixture of clay-size clay minerals and various opaque crystals. Left = plane-polarized light, right = cross-polarized light.

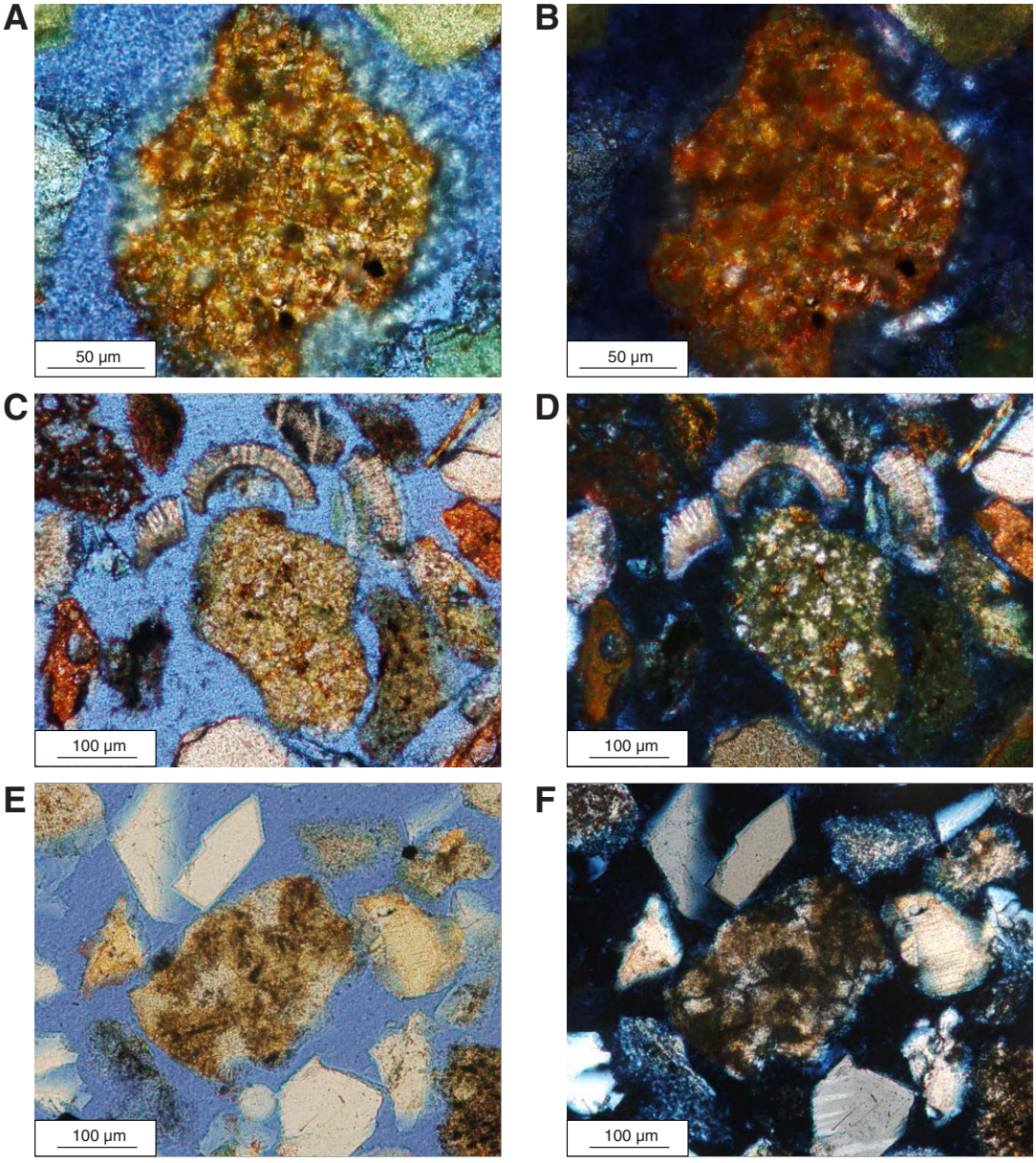

Figure F11. Volcanic rock fragments: felsitic grains are characterized by microcrystalline quartz and feldspar crystals of equant dimensions. The presence of abundant feldspar is denoted by the prominent yellow stain. These grains also contain a substantial admixture of clay-size clay minerals and various opaque crystals. Left = plane-polarized light, right = cross-polarized light.

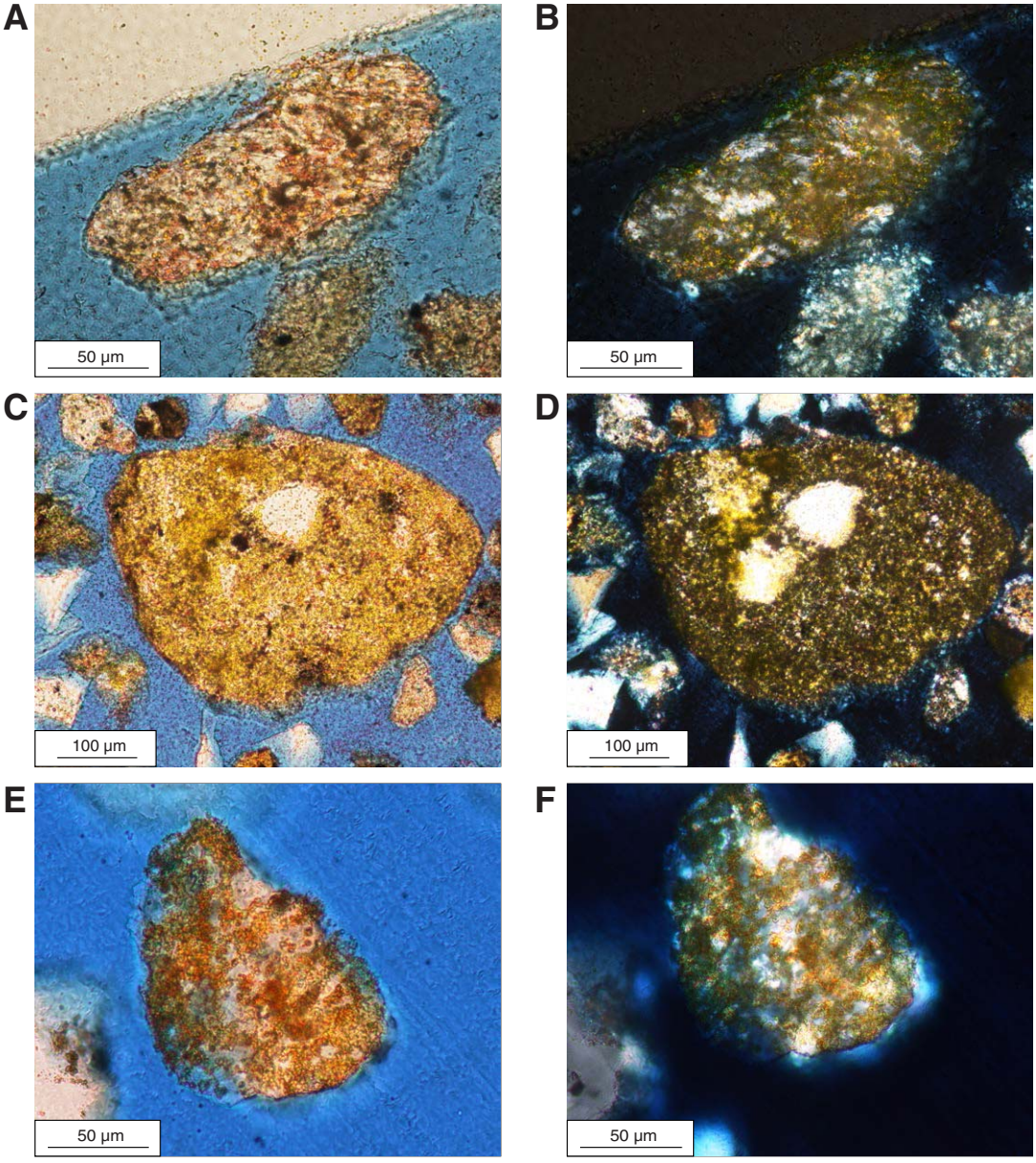

Figure F12. Volcanic rock fragments: microlitic grains containing distinct microcrystals of feldspars floating in a finer grained groundmass of variable feldspar and quartz content. **A, B.** Note the unstained microliths, probable albitic plagioclase. Left = plane-polarized light, right = cross-polarized light.

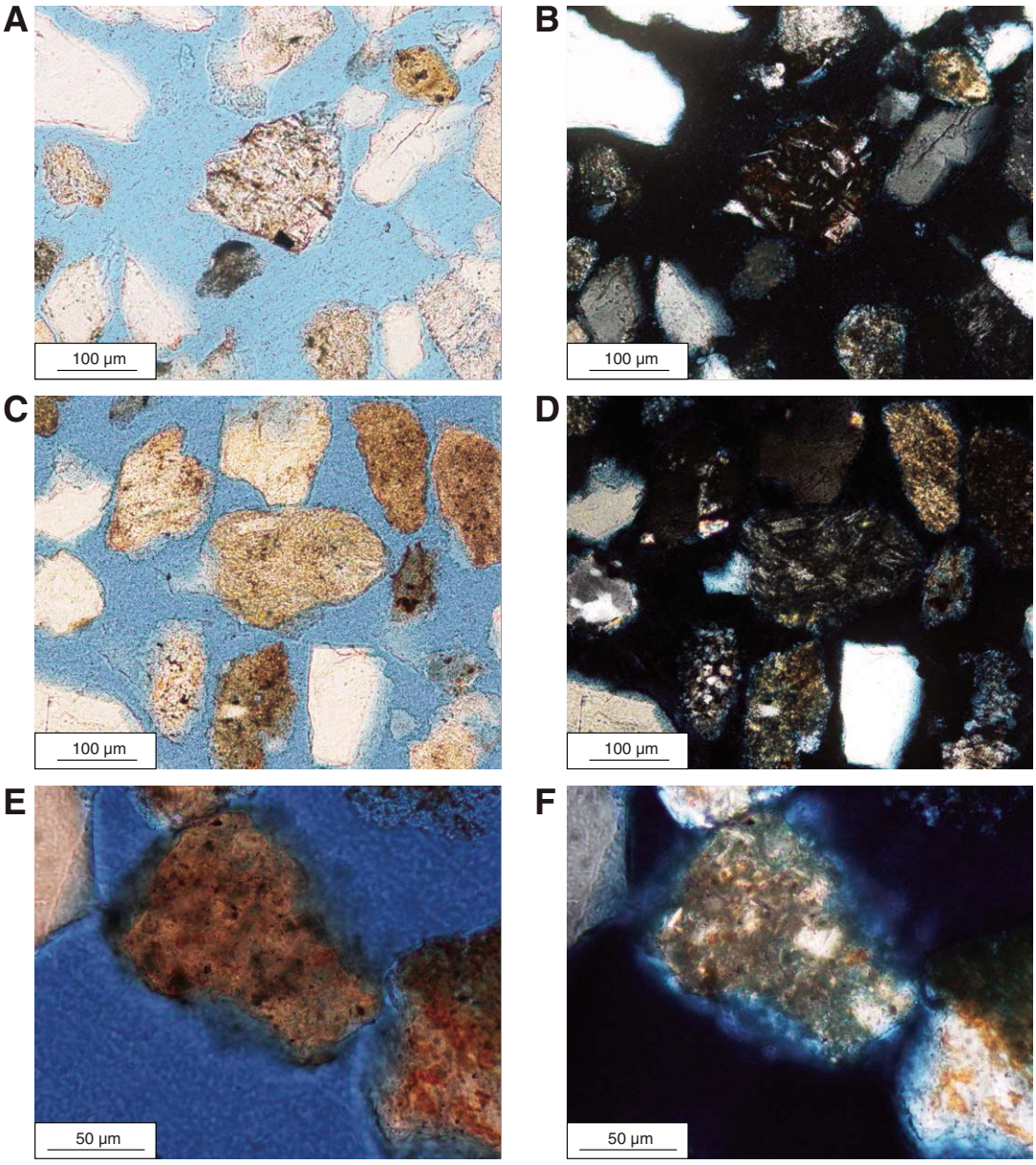

Figure F13. Volcanic rock fragments: lathwork. **A, B, E, F.** Highly altered grains. **C, D.** Note the unstained microliths, probable albitic plagioclase. Left = plane-polarized light, right = cross-polarized light.

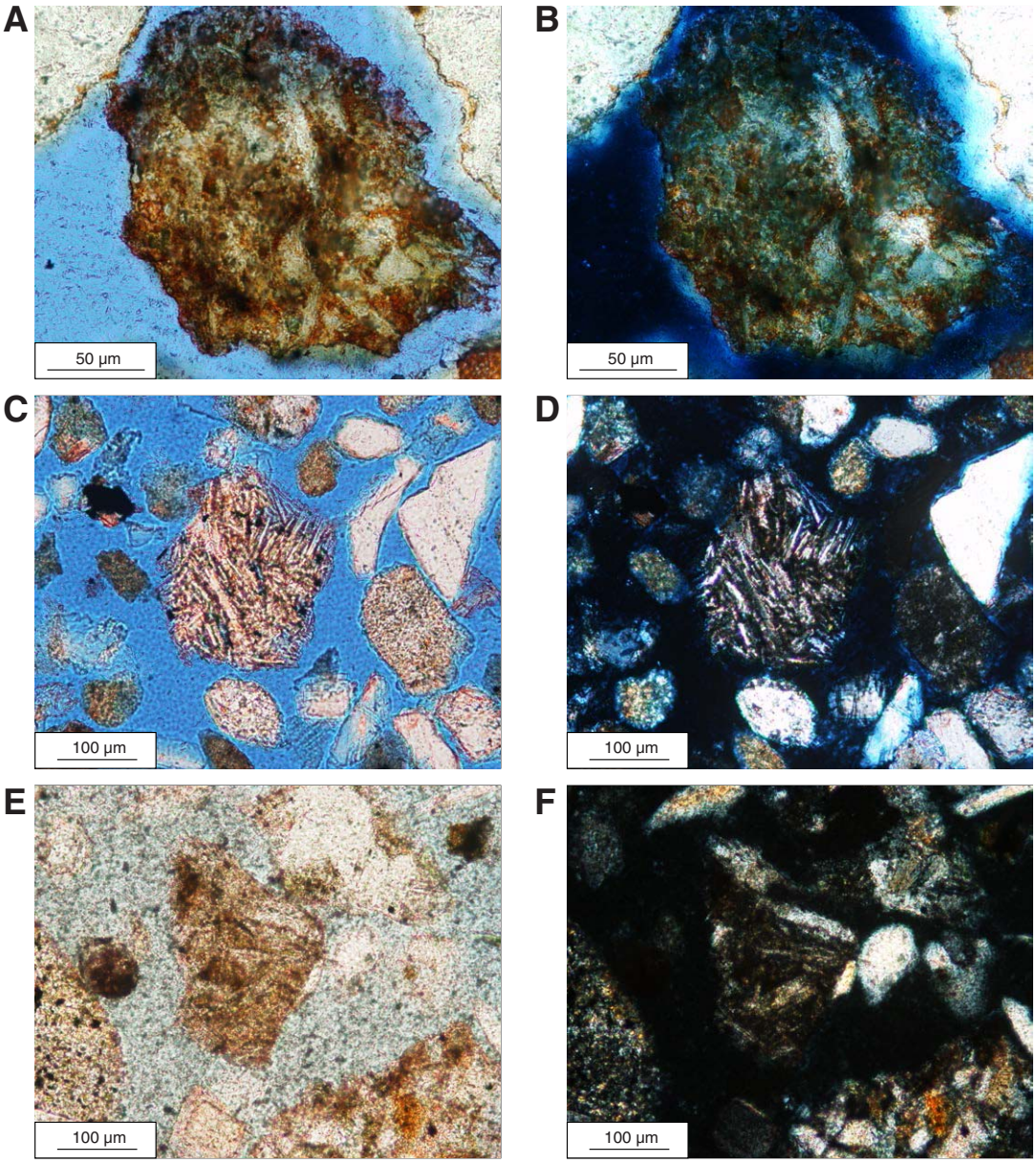

Figure F14. Volcanic rock fragments: trachytic lathwork. Lath crystals are plagioclase. **E, F.** Note dual K-feldspar and plagioclase staining in the groundmass. Left = plane-polarized light, right = cross-polarized light.

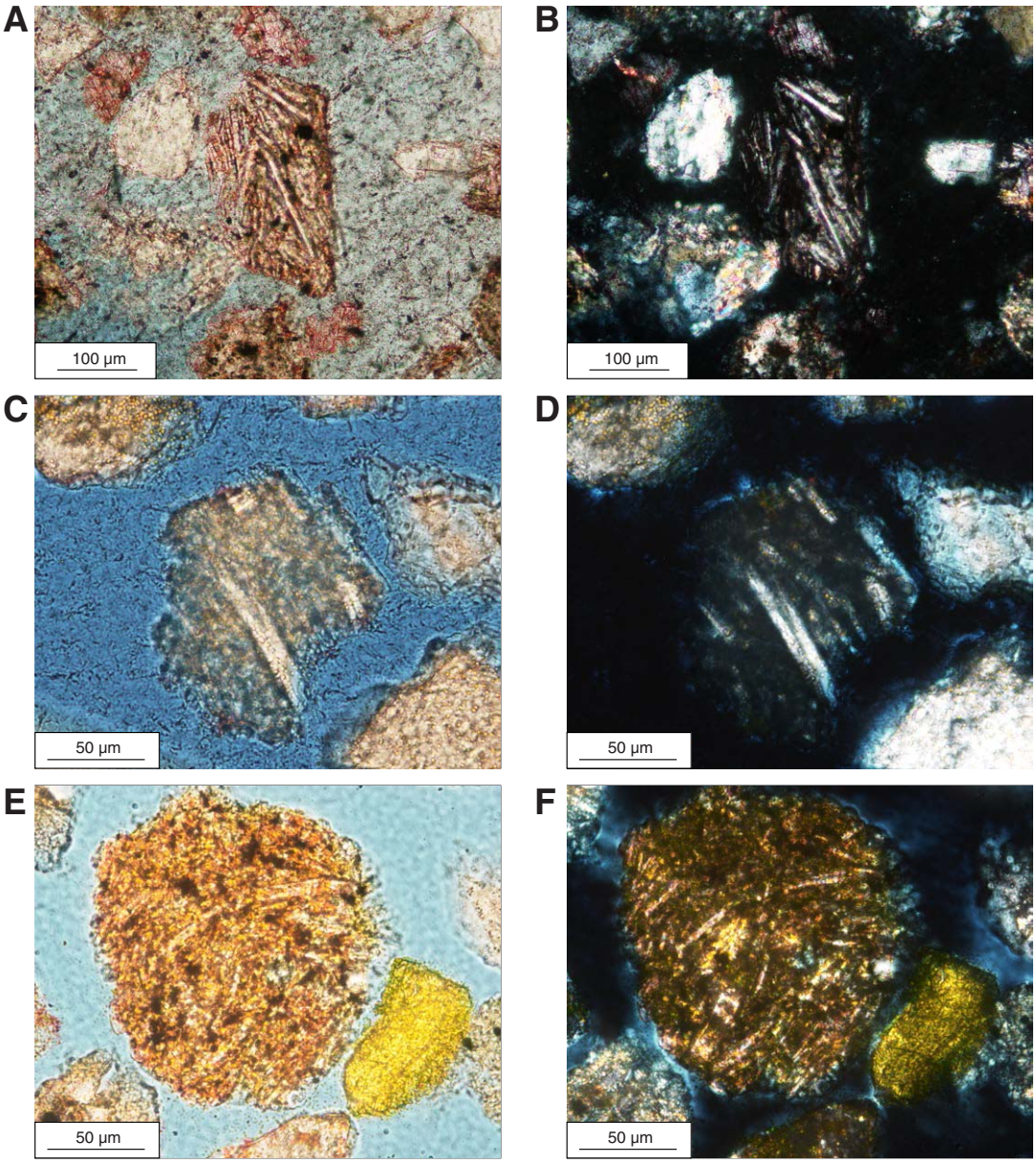

Figure F15. Volcanic rock fragments: pumice, increasing degree of devitrification. Note the microcrystalline quartz-filled vesicle in **E** and **F**. Left = plane-polarized light, right = cross-polarized light.

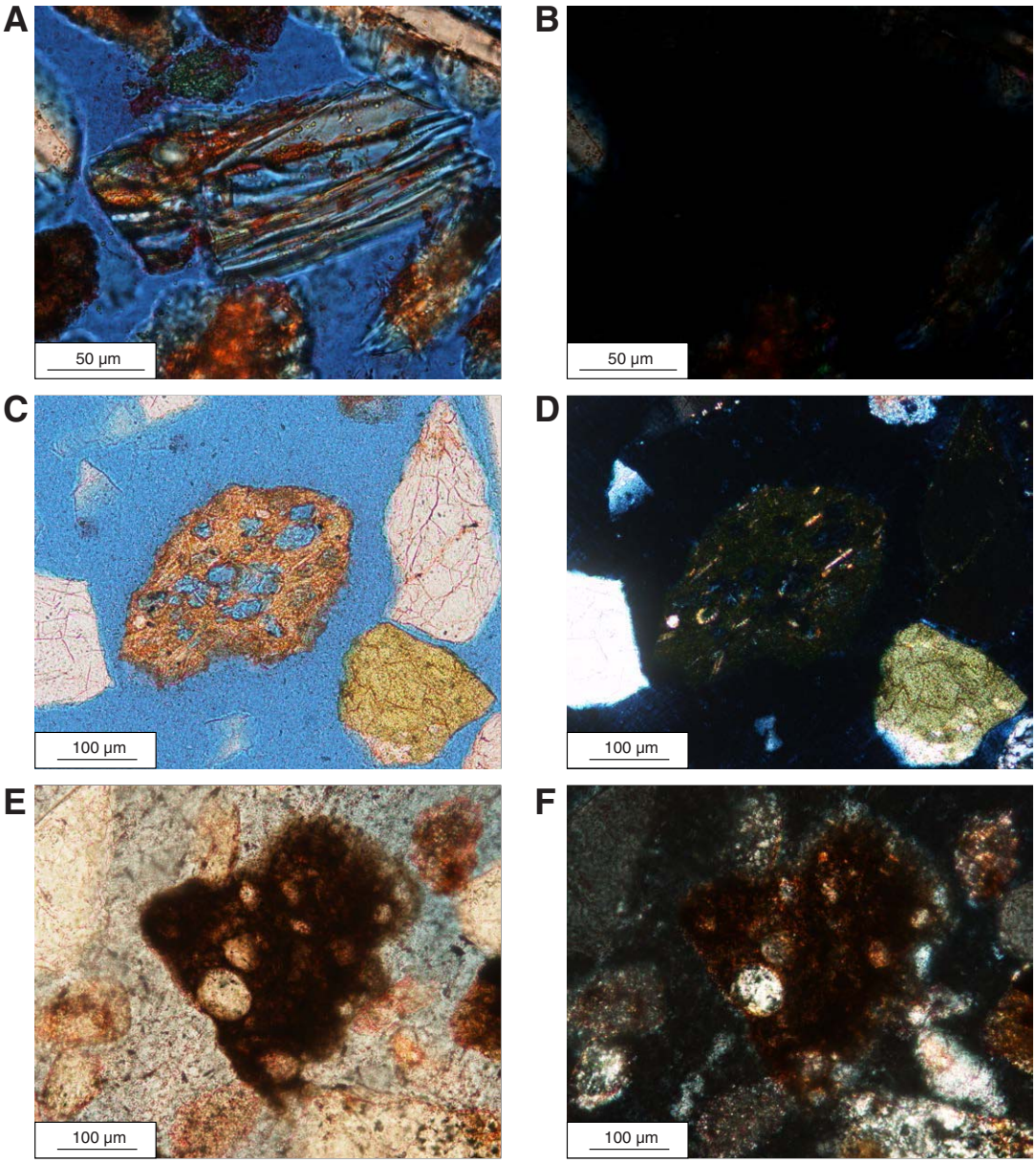

Figure F16. Plutonic rock fragments: quartz-plagioclase-k-feldspar aggregates. Feldspars denoted by staining. Left = plane-polarized light, right = cross-polarized light.

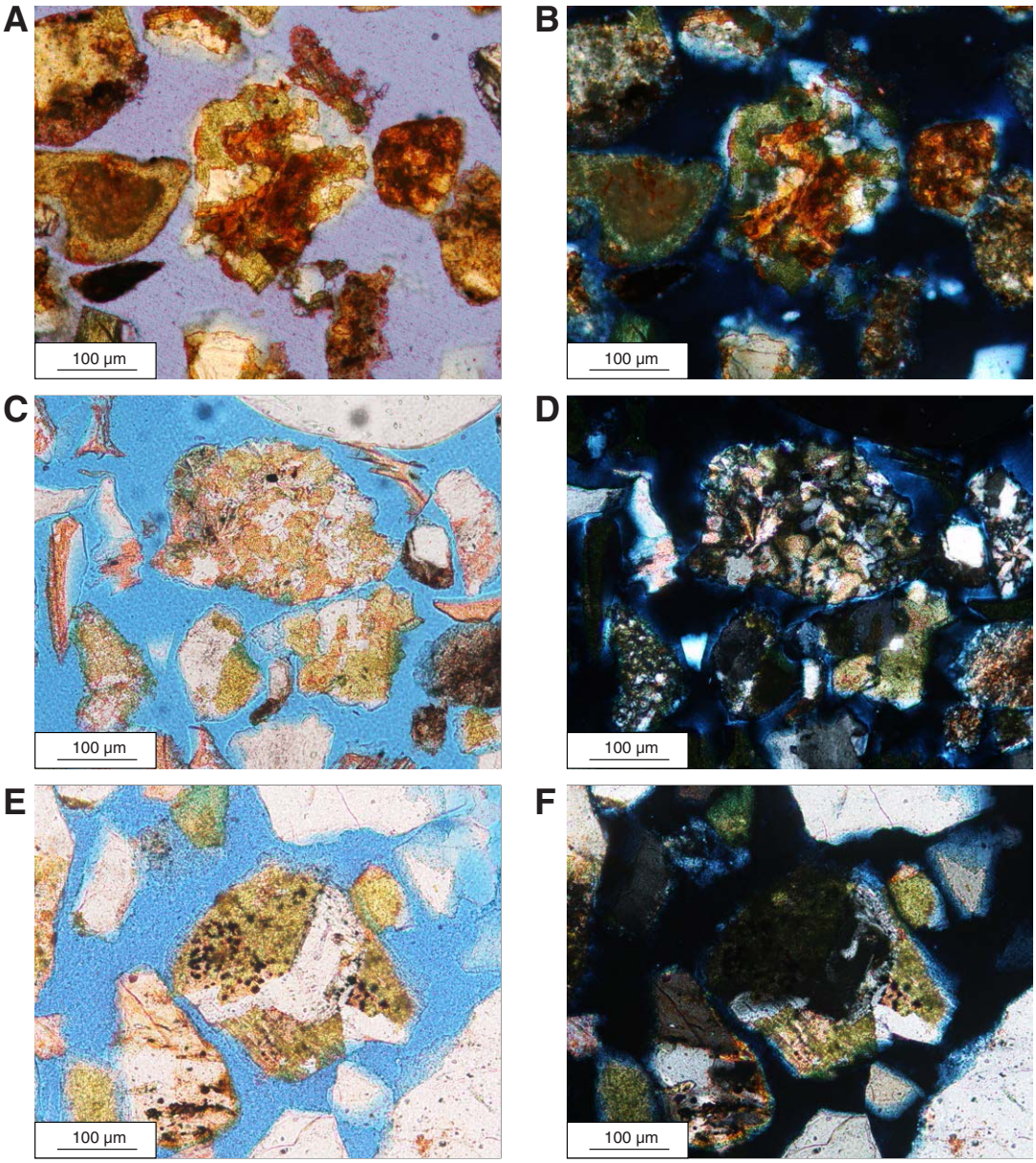

Figure F17. Plutonic rock fragments. **C, D, E, F.** Note carbonate alteration on feldspars. For C and D, alternative interpretation would be carbonate-altered sandstone clast, however, sedimentary fabrics are not clear. Left = plane-polarized light, right = cross-polarized light.

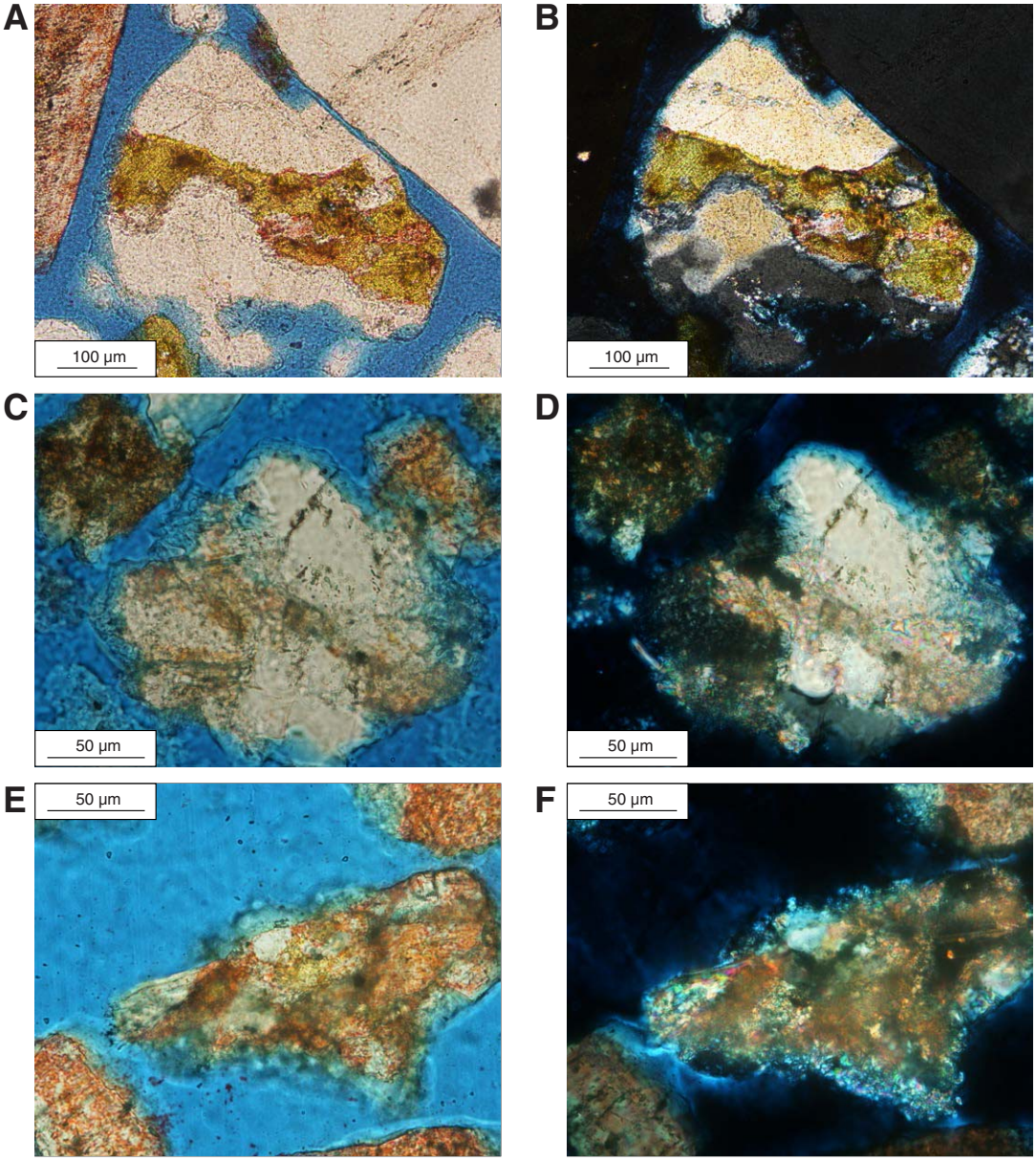

Figure F18. Plutonic rock fragments: quartz-K-feldspar intergrowths. Left = plane-polarized light, right = cross-polarized light.

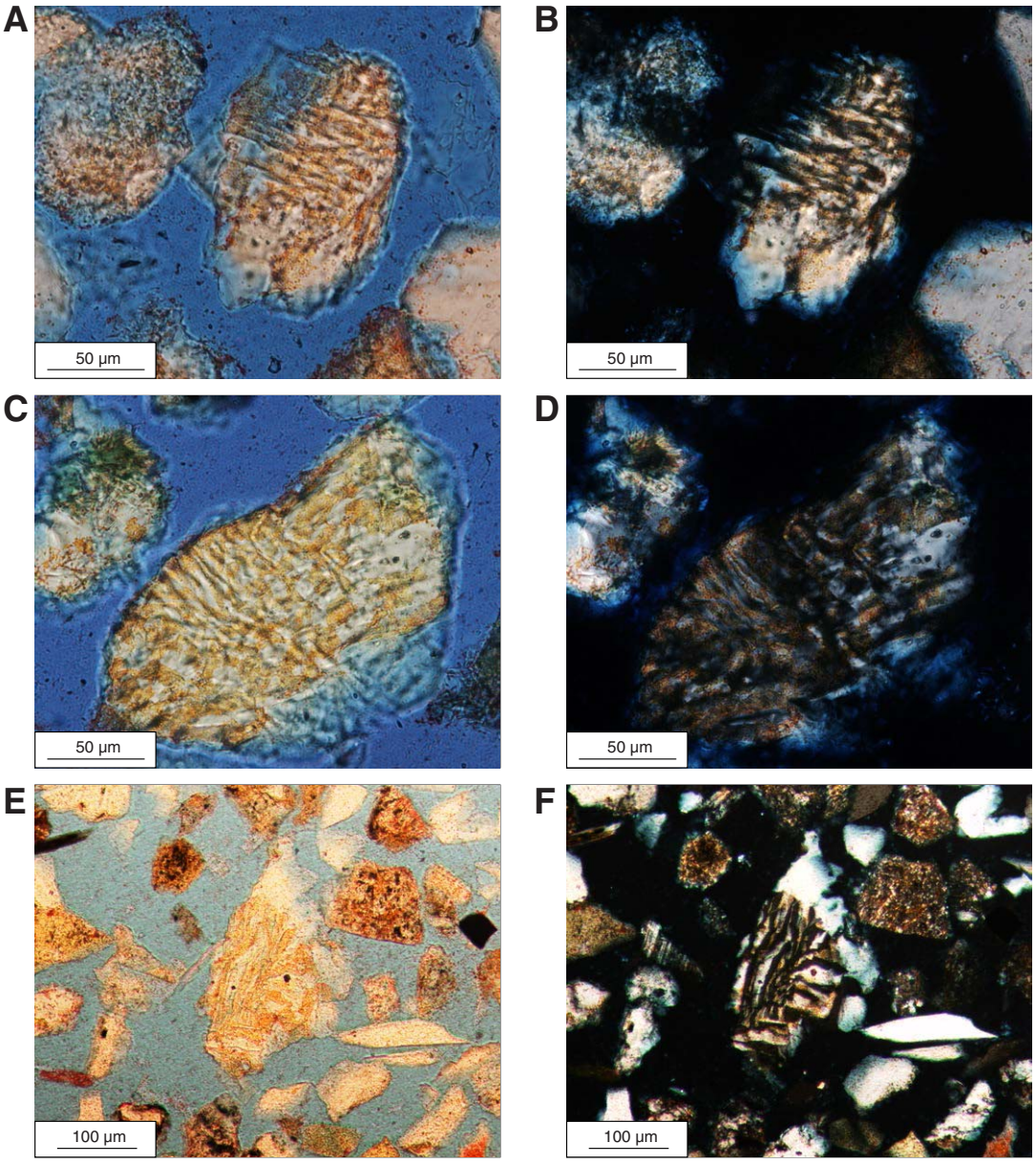

Figure F19. Plutonic rock fragments. **A, B.** Quartz-muscovite aggregate. **C, D.** Quartz-plagioclase aggregate. **E, F.** Quartz-epidote-plagioclase (albite) aggregate. Left = plane-polarized light, right = cross-polarized light.

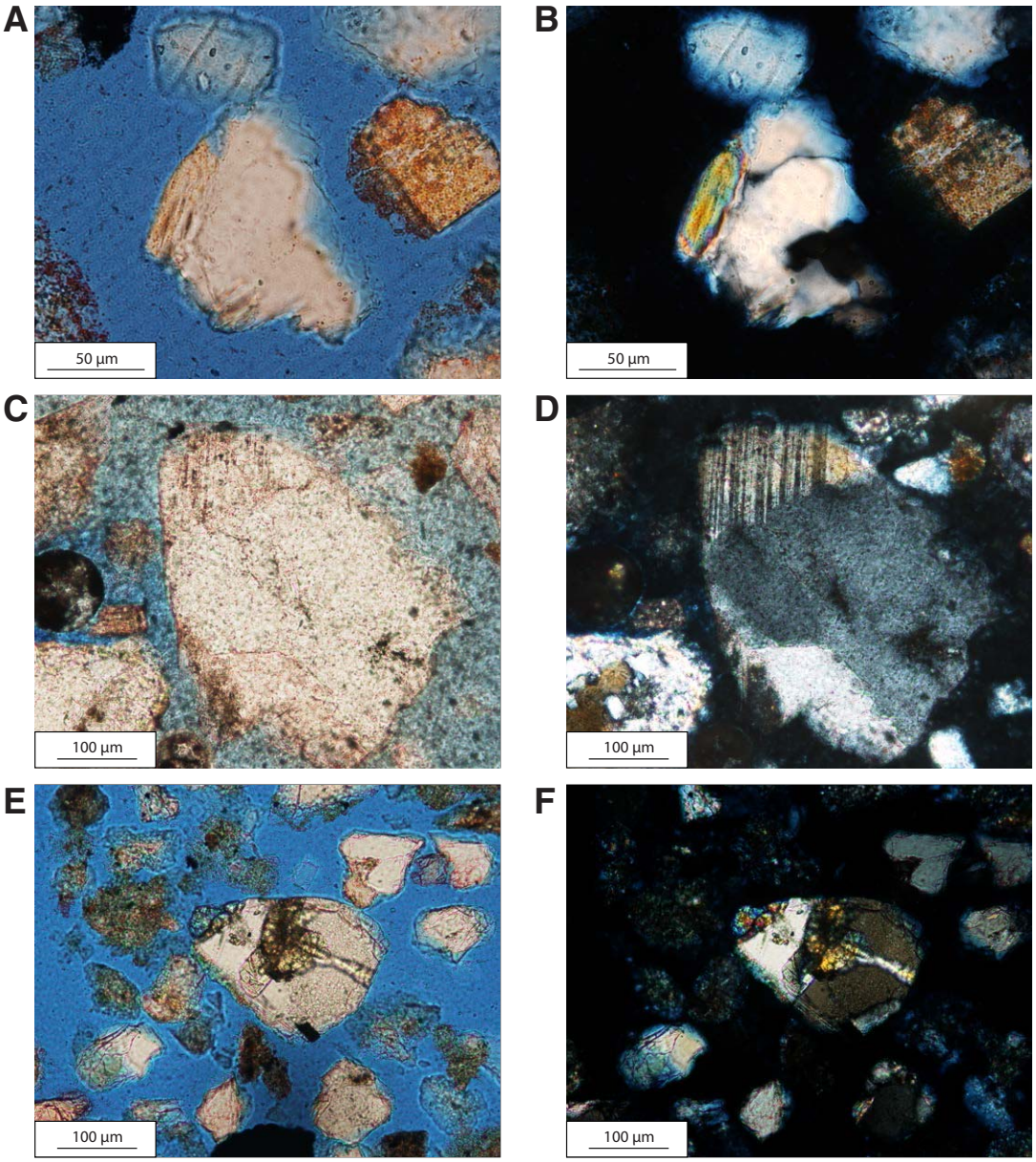

Figure F20. Metamorphic rock fragments: quartz-rich, foliated. Left = plane-polarized light, right = cross-polarized light.

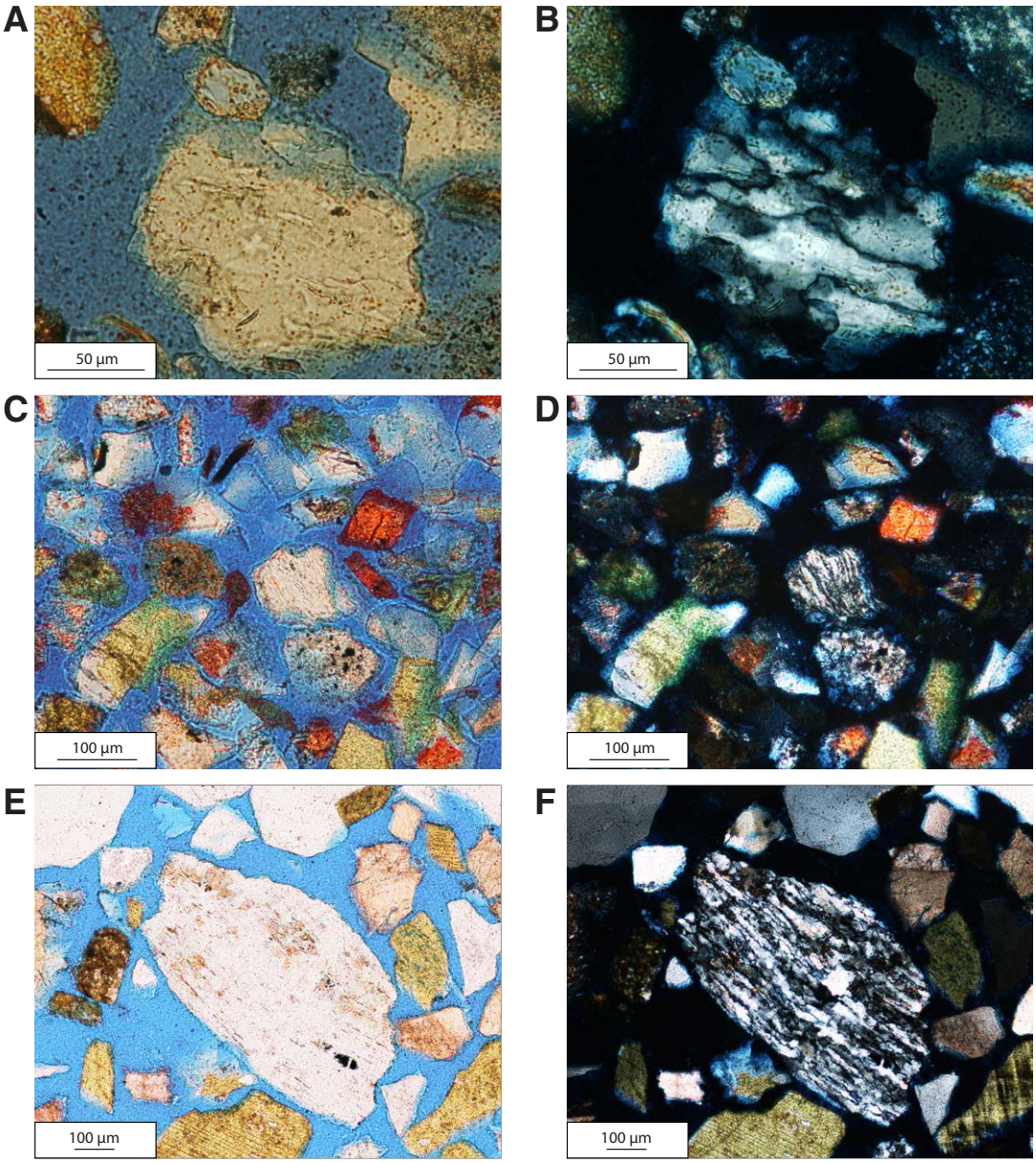

Figure F21. Metamorphic rock fragments: quartz-mica rich, foliated. Left = plane-polarized light, right = cross-polarized light.

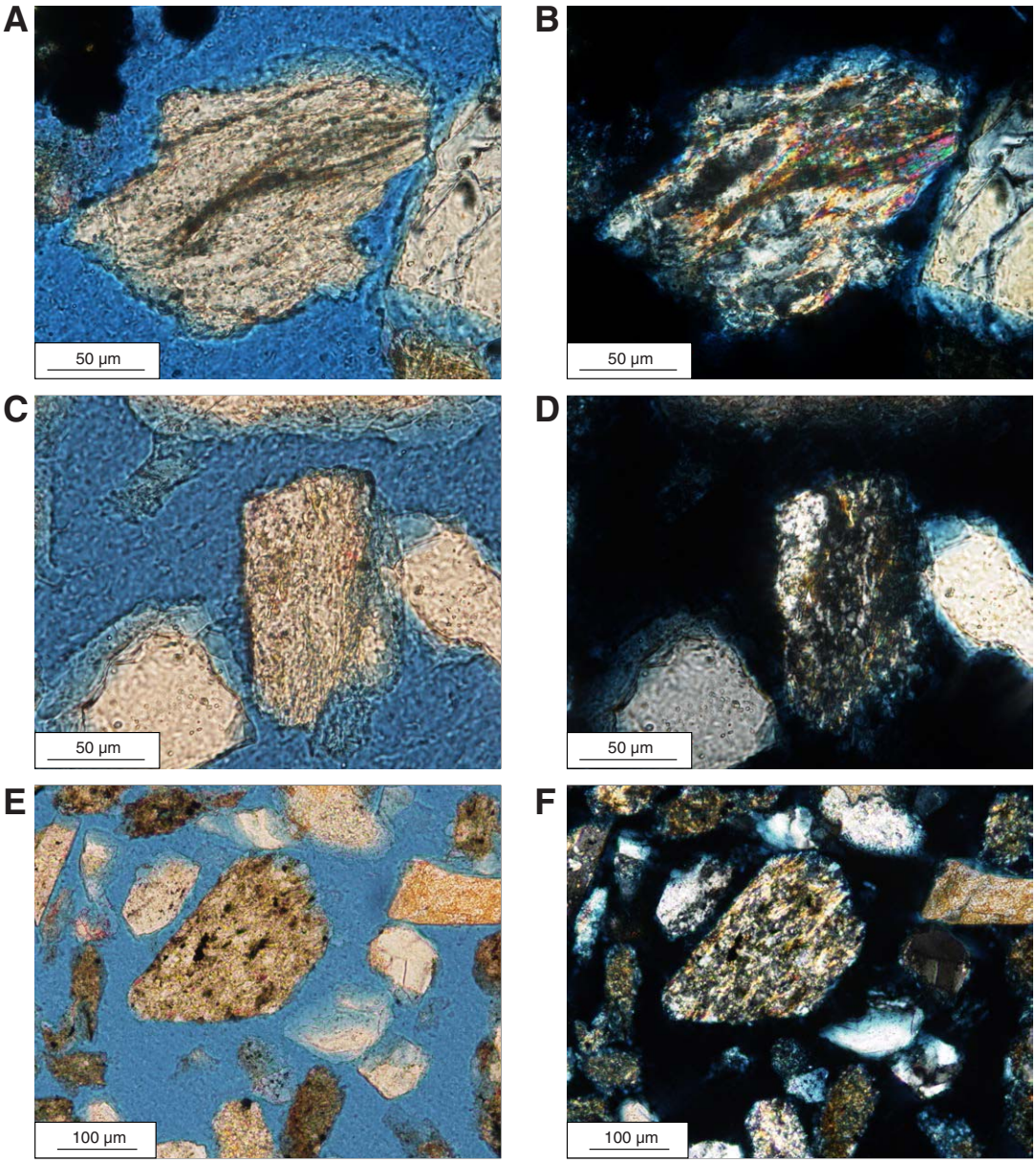

Figure F22. Metamorphic rock fragments: micaceous. Left = plane-polarized light, right = cross-polarized light.

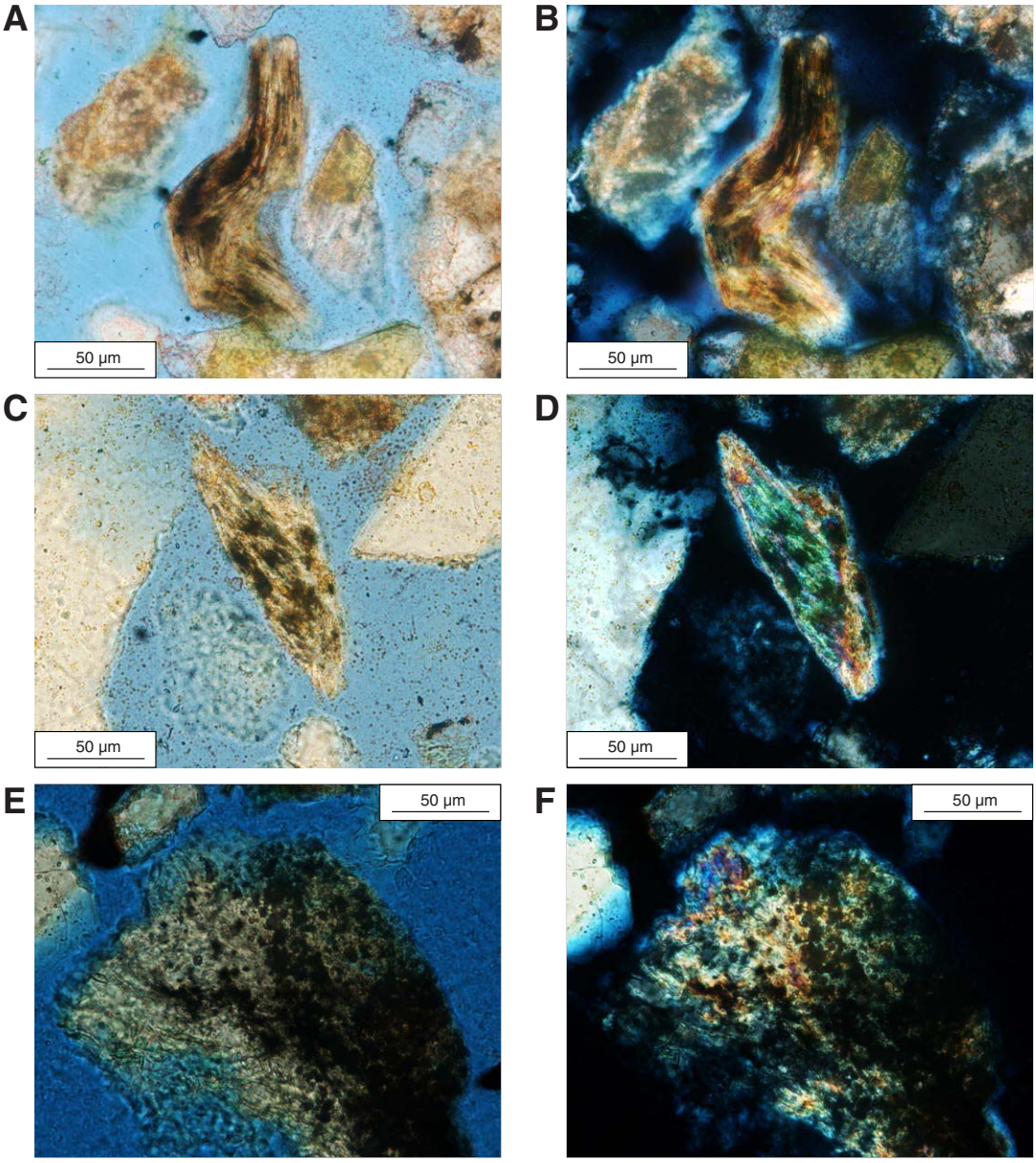

Figure F23. Metamorphic rock fragments: chlorite schists. **E, F.** Alteration has obscured individual chlorite crystals. Left = plane-polarized light, right = cross-polarized light.

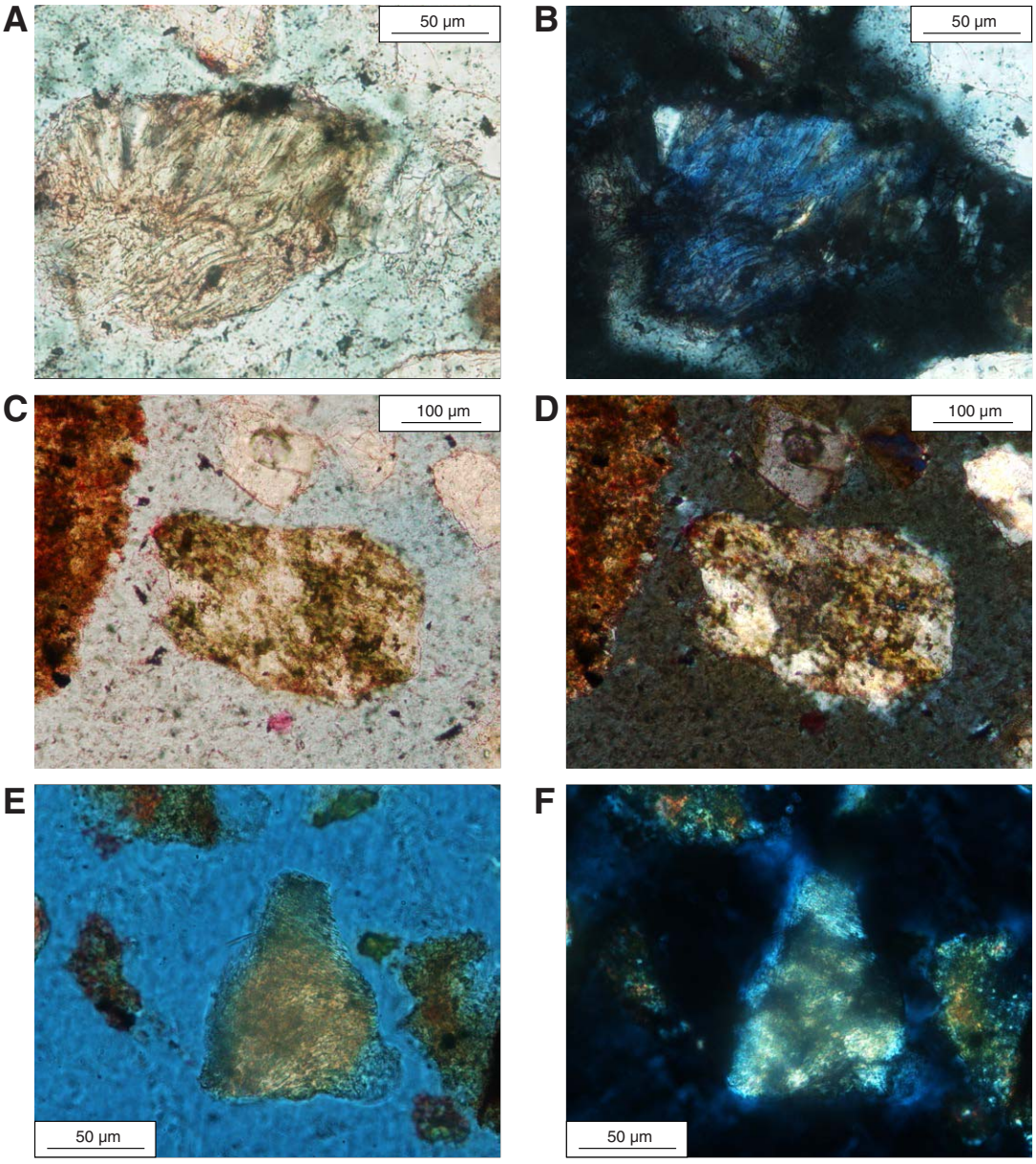

Figure F24. Metamorphic rock fragments: epidote-rich. Left = plane-polarized light, right = cross-polarized light.

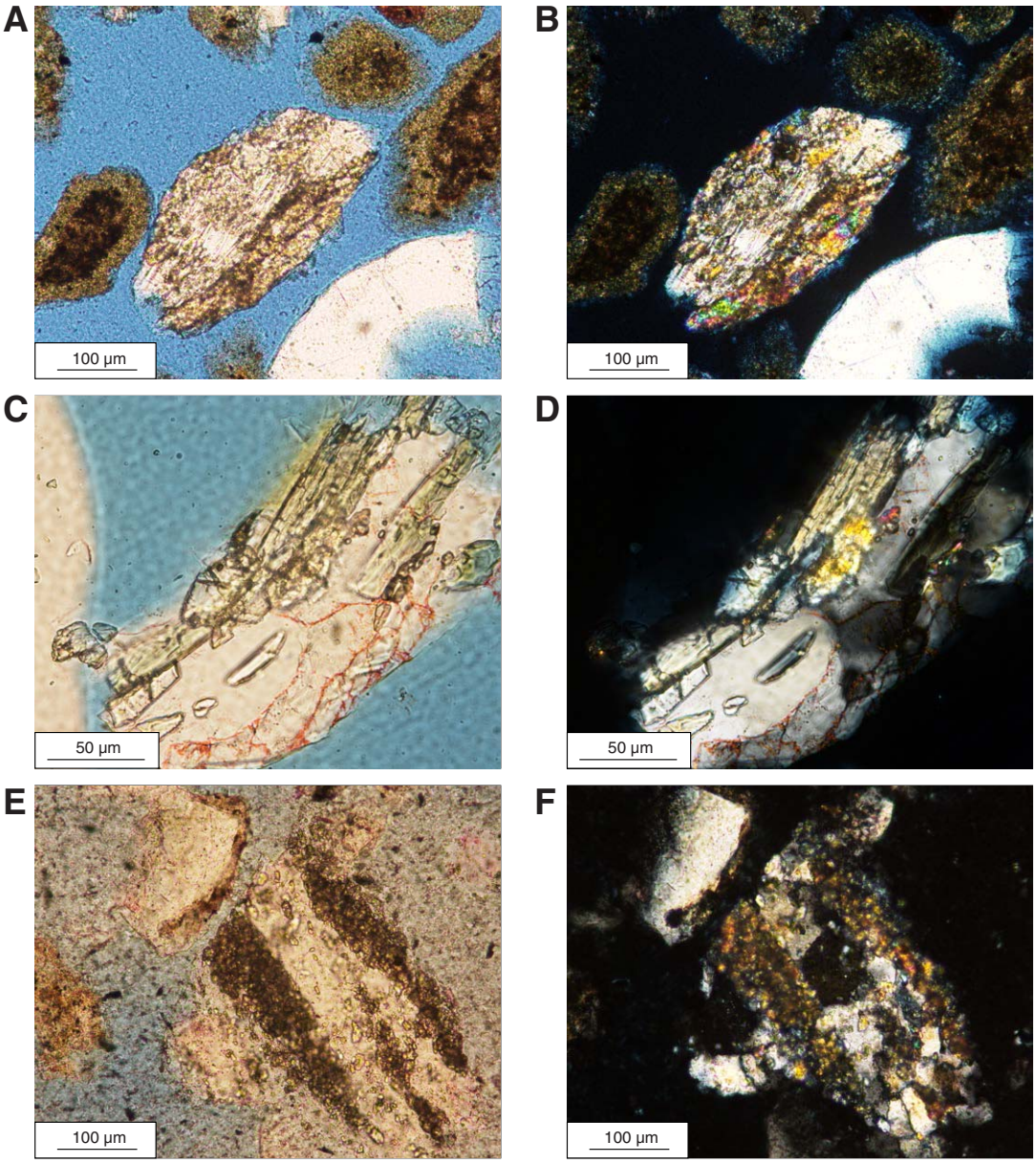

Figure F25. Metamorphic rock fragments. **A, B.** Feldspar-rich, foliated. **C, D.** Quartz-carbonate-mica aggregate, nonfoliated. Lack of foliation would also be consistent with the alternative interpretation of carbonate-altered plutonic rock fragments. **E, F.** Low-grade metamorphic rock fragment (slate) or, alternatively, a fissile silty mudstone. Left = plane-polarized light, right = cross-polarized light.

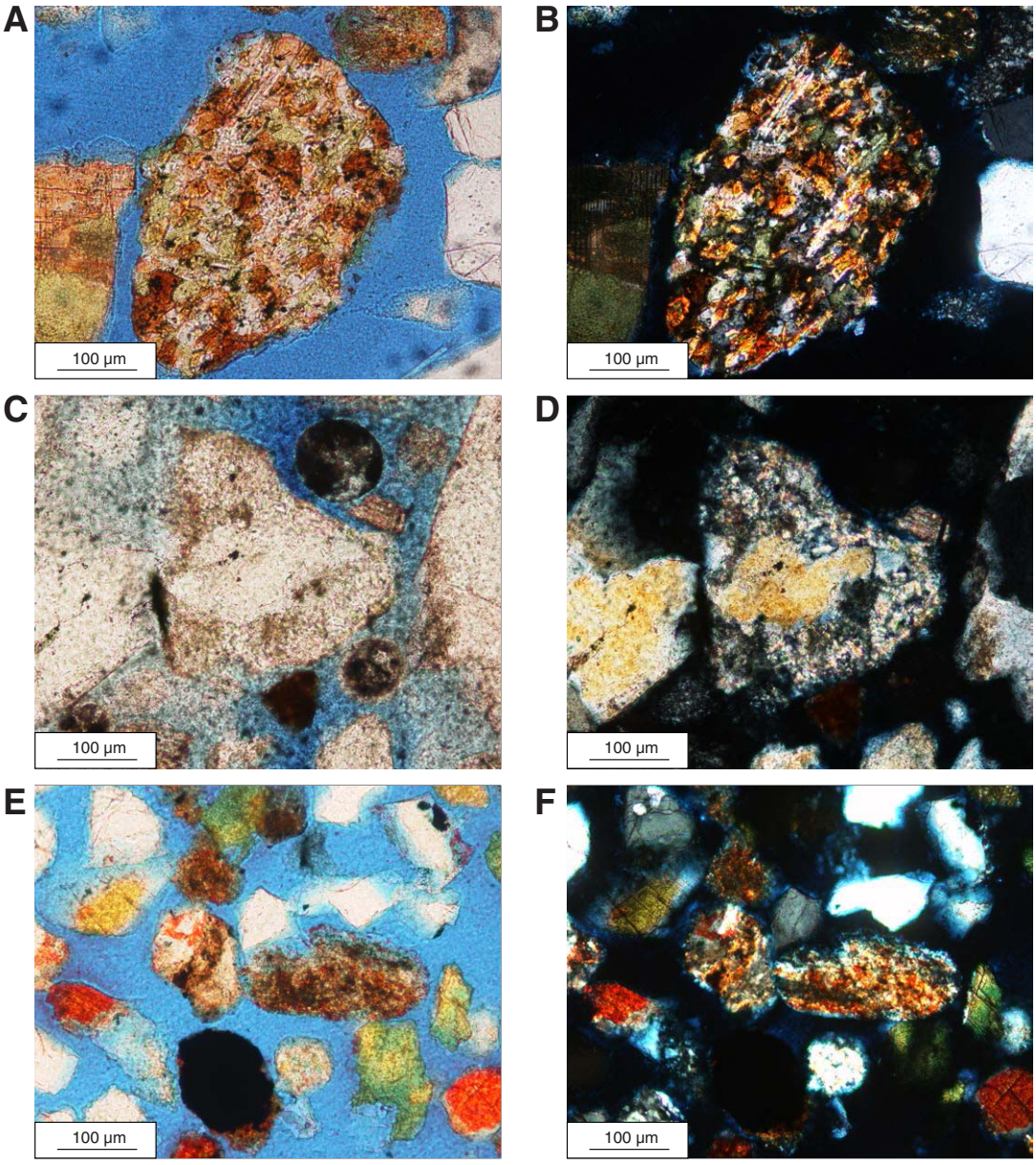

Figure F26. Artifacts: undisaggregated silty mud grains. This interpretation is supported by the size of these fragments, which far exceeds the sizes of the dominant grains in this sediment. Component grains within these large aggregates are also equivalent in size to the surrounding particles. Left = plane-polarized light, right = cross-polarized light.

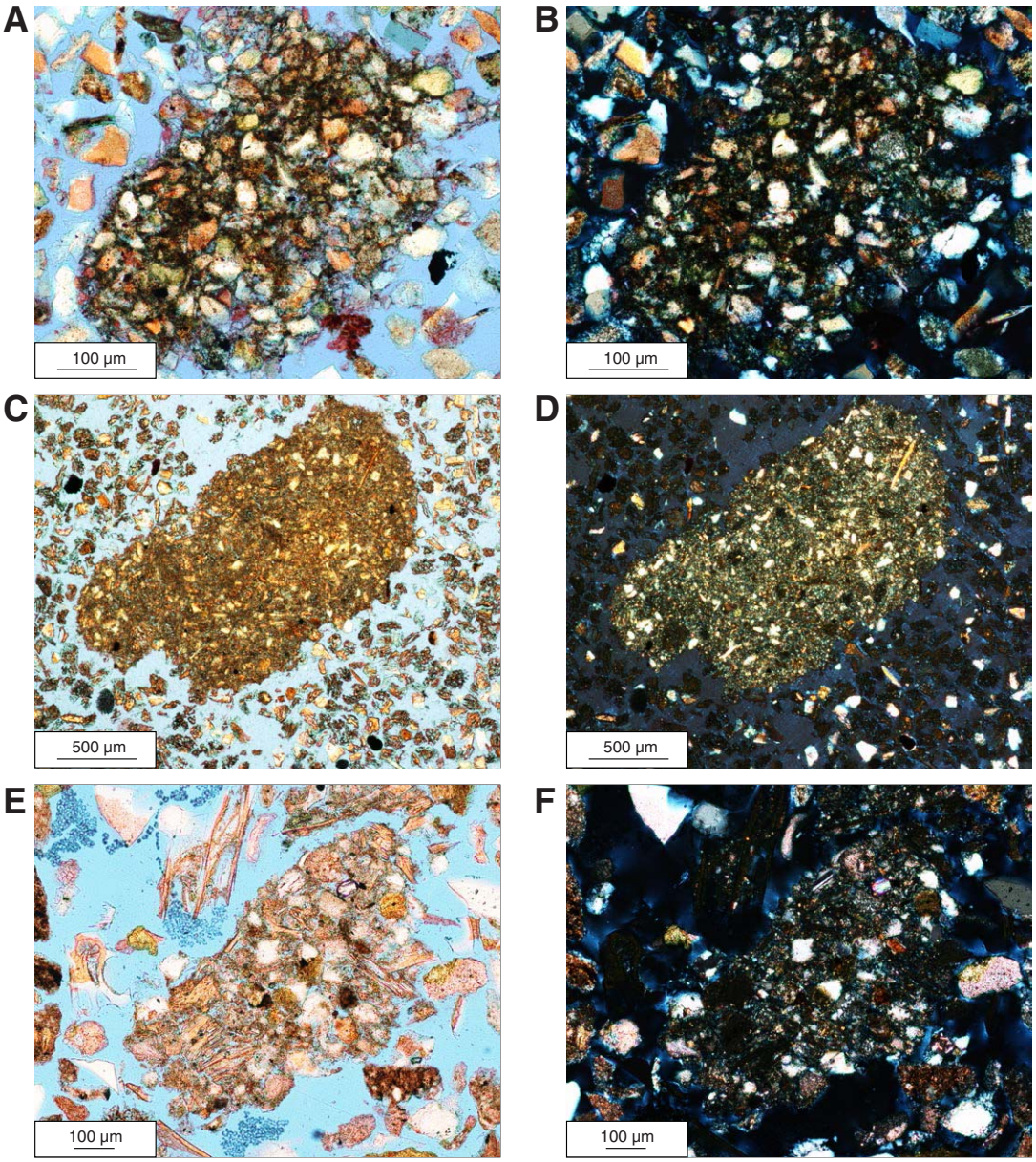

Figure F27. Artifacts: postdrilling sulfate precipitates. Gypsum saturation is not normally expected in the sulfate-poor fluids of the Nankai margin (see fig. F10 in Milliken et al. [2012] for further explanations). Left = plane-polarized light, right = cross-polarized light.

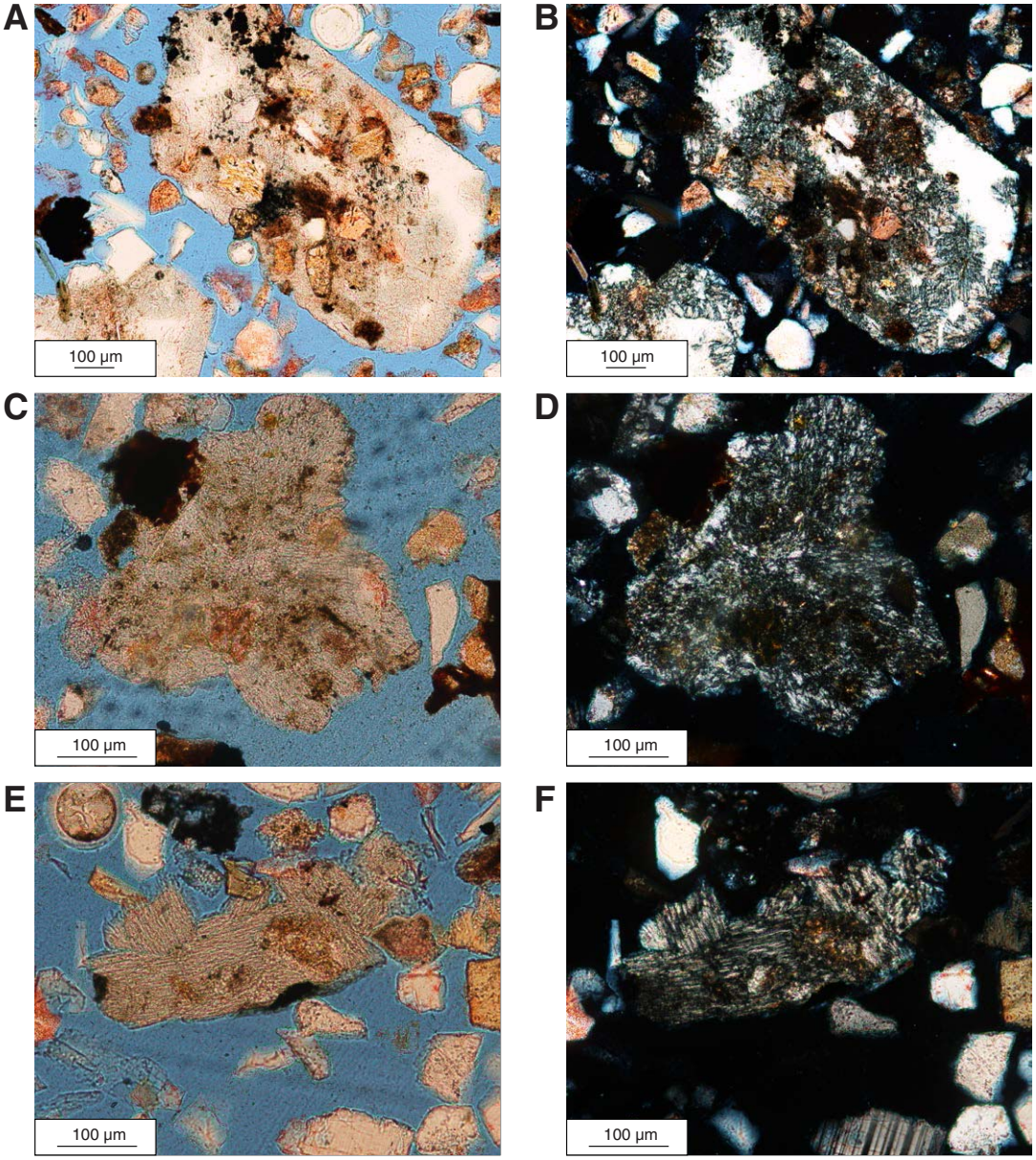

Table T1. Photographed grains shown in figures. (Continued on next page.)

Figure	Lithic grain type	Sample number/ Expedition, hole, core, section, interval (cm)	Unit
F1A, F1B	SRF (mudstone, clay rich)	338-C0002F-215-SMW	V
F1C, F1D	SRF (mudstone, clay rich)	315-C0002D-5H-5, 35–37	I
F1E, F1F	SRF (mudstone, clay rich)	338-C0002L-4X-CC, 36–37.5	II
F2A, F2B	SRF (mudstone, clay rich)	338-C0002F-213-SMW	IV
F2C, F2D	SRF (mudstone, clay rich)	338-C0002L-13X-1, 15–16.5	II
F2E, F2F	SRF (mudstone, clay rich)	315-C0002D-7H-7, 75–77	I
F3A, F3B	SRF (mudstone, clay rich)	338-C0002J-6R-1, 62–63.5	IV
F3C, F3D	SRF (mudstone, clay rich)	338-C0002F-42-SMW	III
F3E, F3F	SRF (mudstone, clay rich)	338-C0002L-9X-7, 79.5–81	II
F4A, F4B	SRF (mudstone, clay rich)	338-C0002F-58 SMW	IV
F4C, F4D	SRF (mudstone, clay rich)	338-C0002L-16X-5, 64–65	II
F4E, F4F	SRF (mudstone, clay rich)	315-C0002D-14H-4, 81–83	I
F5A, F5B	SRF (mudstone, clay rich)	338-C0002K-6T-3, 20–21.5	II
F5C, F5D	SRF (mudstone, clay rich)	338-C0002K-7X-3, 30–31.5	I
F5E, F5F	SRF (mudstone, clay rich)	315-C0002D-14H-4, 81–83	I
F6A, F6B	SRF (mudstone, silt rich)	338-C0002F-58-SMW	IV
F6C, F6D	SRF (mudstone, silt rich)	338-C0002F-68-SMW	IV
F6E, F6F	SRF (mudstone, silt rich)	338-C0002F-58-SMW	IV
F7A, F7B	SRF (mudstone, silt rich)	338-C0002F-233-SMW	V
F7C, F7D	SRF (mudstone, silt rich)	338-C0002K-6T-3, 20–21.5	II
F7E, F7F	SRF (sandstone)	338-C0002F-77-SMW	IV
F8A, F8B	SRF (argillaceous chert)	315-C0002B-63R-1, 74–76	IV
F8C, F8D	SRF (argillaceous chert)	338-C0002F-120-SMW	IV
F8E, F8F	SRF (argillaceous chert)	338-C0002F-161-SMW	IV
F9A, F9B	SRF (chert)	338-C0002F-84-SMW	IV
F9C, F9D	SRF (chert)	315-C0002B-1R-3, 125–127	II
F9E, F9F	SRF (chert)	338-C0002J-6R-1, 62–63.5	IV
F10A, F10B	VRF (felsitic)	315-C0002D-11H-6, 108–110	I
F10C, F10D	VRF (felsitic)	315-C0002D-11H-6, 108–110	I
F10E, F10F	VRF (felsitic)	338-C0002K-5T-1, 30–31.5	II
F11A, F11B	VRF (felsitic)	338-C0002F-51-SMW	IV
F11C, F11D	VRF (felsitic)	338-C0002F-77-SMW	IV
F11E, F11F	VRF (felsitic)	338-C0002-F-233-SMW	V
F12A, F12B	VRF (microlitic)	338-C0002L-22X-7, 39–40	II
F12C, F12D	VRF (microlitic)	338-C0002F-58-SMW	IV
F12E, F12F	VRF (microlitic)	338-C0002-F-233-SMW	V
F13A, F13B	VRF (lathwork)	315-C0002D-8H-2, 27–29	I
F13C, F13D	VRF (lathwork)	338-C0002F-42-SMW	III
F13E, F13F	VRF (lathwork)	315-C0002B-63R-1, 74–76	IV
F14A, F14B	VRF (trachytic lathwork)	315-C0002B-59R-1, 33–35	IV
F14C, F14D	VRF (trachytic lathwork)	338-C0002F-58-SMW	IV
F14E, F14F	VRF (trachytic lathwork)	338-C0002F-98-SMW	IV
F15A, F15B	VRF (pumice)	338-C0002L-6X-6, 26–28	II
F15C, F15D	VRF (pumice)	315-C0002B-14R-1, 112–114	II
F15E, F15F	VRF (pumice)	315-C0002B-59R-1, 33–35	IV
F16A, F16B	PRF	315-C0002D-8H-2, 27–29	I
F16C, F16D	PRF	315-C0002B-14R-1, 112–114	II
F16E, F16F	PRF	338-C0002J-6R-1, 62–63.5	IV
F17A, F17B	PRF	338-C0002F-90-SMW	IV
F17C, F17D	PRF	338-C0002F-209-SMW	IV
F17E, F17F	PRF	338-C0002F-213-SMW	IV
F18A, F18B	PRF (quartz-K-feldspar intergrowth)	338-C0002K-3T-CC, 25.5–27	II
F18C, F18D	PRF (quartz-K-feldspar intergrowth)	338-C0002K-5T-1, 30–31.5	II
F18E, F18F	PRF (quartz-K-feldspar intergrowth)	338-C0002L-16X-5, 64–65	II
F19A, F19B	PRF	338-C0002K-3T-CC, 25.5–27	II
F19C, F19D	PRF	315-C0002B-63R-1, 74–76	IV
F19E, F19F	PRF	338-C0002F-51-SMW	IV
F20A, F20B	MRF (quartz rich)	338-C0002K-11X-4, 10–11.5	II
F20C, F20D	MRF (quartz rich)	338-C0002L-24X-6, 67–68	II
F20E, F20F	MRF (quartz rich)	338-C0002J-6R-1, 62–63.5	IV
F21A, F21B	MRF (quartz-mica rich)	338-C0002F-51-SMW	IV
F21C, F21D	MRF (quartz-mica rich)	338-C0002F-58-SMW	IV
F21E, F21F	MRF (quartz-mica rich)	338-C0002F-120-SMW	IV
F22A, F22B	MRF (micaceous)	315-C0002D-5H-5, 35–37	I
F22C, F22D	MRF (micaceous)	338-C0002K-11X-4, 10–11.5	II
F22E, F22F	MRF (micaceous)	338-C0002F-182-SMW	IV
F23A, F23B	MRF (chlorite rich)	338-C0002F-174-SMW	IV
F23C, F23D	MRF (chlorite rich)	338-C0002F-199-SMW	IV

Table T1 (continued).

Figure	Lithic grain type	Sample number/ Expedition, hole, core, section, interval (cm)	Unit
F23E, F23F	MRF (chlorite rich)	338-C0002F-213-SMW	IV
F24A, F24B	MRF (epidote rich)	338-C0002F-68-SMW	IV
F24C, F24D	MRF (epidote rich)	338-C0002F-98-SMW	IV
F24E, F24F	MRF (epidote rich)	338-C0002F-110-SMW	IV
F25A, F25B	MRF (other)	338-C0002J-6R-1, 62–63.5	IV
F25C, F25D	MRF (other)	315-C0002B-63R-1, 74–76	IV
F25E, F25F	MRF (other)	338-C0002F-250-SMW	V
F26A, F26B	Artifact (undisaggregated mud)	338-C0002L-9X-7, 79.5–81	II
F26C, F26D	Artifact (undisaggregated mud)	338-C0002L-13X-6, 71–72.5	II
F26E, F26F	Artifact (undisaggregated mud)	315-C0002B-14R-1, 112–114	II
F27A, F27B	Artifact (sulfate precipitate)	338-C0002L-19X-7, 06–07	II
F27C, F27D	Artifact (sulfate precipitate)	338-C0002L-20X-CC, 46–47	II
F27E, F27F	Artifact (sulfate precipitate)	338-C0002L-20X-CC, 46–47	II

SRF = sedimentary lithic fragment, VRF = volcanic lithic fragment, PRF = plutonic lithic fragment, MRF = metamorphic lithic fragment.